Hsp90 induces increased genomic instability toward DNA-damaging agents by tuning down *RAD53* transcription

Nidhi Khurana[a], Shyamasree Laskar[a], Mrinal K. Bhattacharyya[b], and Sunanda Bhattacharyya[a,*]
[a]Department of Biotechnology and Bioinformatics and [b]Department of Biochemistry, School of Life Sciences, University of Hyderabad, Hyderabad 500046, India

ABSTRACT **It is well documented that elevated body temperature causes tumors to regress upon radiotherapy. However, how hyperthermia induces DNA damage sensitivity is not clear. We show that a transient heat shock and particularly the concomitant induction of Hsp90 lead to increased genomic instability under DNA-damaging conditions. Using *Saccharomyces cerevisiae* as a model eukaryote, we demonstrate that elevated levels of Hsp90 attenuate efficient DNA damage signaling and dictate preferential use of the potentially mutagenic double-strand break repair pathway. We show that under normal physiological conditions, Hsp90 negatively regulates *RAD53* transcription to suppress DNA damage checkpoint activation. However, under DNA damaging conditions, *RAD53* is derepressed, and the increased level of Rad53p triggers an efficient DNA damage response. A higher abundance of Hsp90 causes increased transcriptional repression on *RAD53* in a dose-dependent manner, which could not be fully derepressed even in the presence of DNA damage. Accordingly, cells behave like a *rad53* loss-of-function mutant and show reduced NHEJ efficiency, with a drastic failure to up-regulate *RAD51* expression and manifestly faster accumulation of *CLN1* and *CLN2* in DNA-damaged G1, cells leading to premature release from checkpoint arrest. We further demonstrate that Rad53 overexpression is able to rescue all of the aforementioned deleterious effects caused by Hsp90 overproduction.**

Monitoring Editor
William P. Tansey
Vanderbilt University

Received: Dec 30, 2015
Revised: May 2, 2016
Accepted: Jun 9, 2016

INTRODUCTION

There is considerable evidence that hyperthermia causes tumor regression by sensitizing cells to DNA-damaging agents. The quest for the mechanism behind such a phenotype has led to various studies, which indicate that a short exposure to heat (41–45°C) causes rewiring of the DNA damage checkpoint cascade, leading to cell cycle arrest at G2/M and apoptosis. Delayed activation of ATM at high temperatures is accompanied by relocalization of the Mre11/Rad50/Nbs1 (MRN) complex from the nucleus to the cytoplasm (Seno and Dynlacht, 2004) and prevention of recruitment of 53BP1 to DNA (Hunt *et al.*, 2007; Laszlo and Fleischer, 2009). It has also been observed that upon heat induction, release of the protein nucleolin occurs from the nucleolus, which then binds to replication protein A (RPA), causing reprogramming of ataxia telangiectasia mutated and Rad3–related (ATR) activation. Consequently, despite the presence of other factors such as the Rad9–Rad1–Hus1 ring (9-1-1) and TopBP1 (Daniely and Borowiec, 2000; VanderWaal *et al.*, 2001), ATR fails to modify RPA32 and therefore cannot elicit a potent DNA-damage signaling cascade. This shift in ATM and ATR functions from DNA damage signaling to "heat sensing" at elevated temperature renders cancer cells sensitive to radiation. During the onset of heat shock response by heat shock factors, the cells in most tissues undergo a dramatic increase in the production of a particular class of molecular chaperones termed heat-shock proteins (Hsps). However, whether the overexpression of Hsps is responsible for poor DNA damage sensitivity has not been explored.

This article was published online ahead of print in MBoC in Press (http://www.molbiolcell.org/cgi/doi/10.1091/mbc.E15-12-0867) on June 15, 2016.

The authors declare that they have no conflict of interest.

*Address correspondence to: Sunanda Bhattacharyya (sdeb70@gmail.com).

Abbreviations used: CEN, centromeric; HOcs, homothallic endonuclease cut site; Hsp90, heat shock protein 90; SSA, single-strand annealing.

Among the heat-shock family of proteins, Hsp90 is an evolutionarily conserved molecular chaperone with two paralogues in eukaryotic cells: Hsp90α and Hsp90β. Hsp90β (Hsc82 in yeast) is constitutively expressed in normal cells and constitutes about 1–2% of total cellular protein (Borkovich *et al.*, 1989; Caplan *et al.*, 2003). Hsp90α (Hsp82 in yeast) is constitutively expressed at a very lower level under normal physiological condition and is strongly induced by heat shock. It has been established that Hsp90 directly interacts with and chaperones several important proteins of DNA repair pathway, such as the checkpoint kinase Chk1 (Arlander *et al.*, 2003), BRCA1 (Stecklein *et al.*, 2012), and Rad51 (Suhane *et al.*, 2015). Apart from the traditional chaperone role of Hsp90 in the cytoplasm, it displays a regulatory role in gene expression. It modulates the activity of chromatin modifiers and thereby alters gene expression (Tariq *et al.*, 2009; Laskar *et al.*, 2011, 2015; Khurana and Bhattacharyya, 2015). Studies indicate that Hsp90 controls transcription either by stalling RNA polymerase II (Sawarkar *et al.*, 2012) or removing nucleosome from the transcription start site (TSS; Floer *et al.*, 2008). Hsp90 targets the promoter of about one-third of the *Drosophila* genome, which includes several signal-responsive genes. However, whether Hsp90 is involved in transcriptional control of the DNA damage response pathway remains elusive. Any such regulation, if proved, would be beneficial for better understanding the DNA repair pathway, which is the central component of tumor growth and maintenance.

Poor genomic integrity is attributed to an ineffective DNA repair mechanism. The DNA damage response pathway comprises two main stages: 1) a DNA damage signaling cascade and 2) DNA repair. DNA damage is initially sensed via a set of sensor proteins, which include the Mre11/Rad50/Xrs2 complex in *Saccharomyces cerevisiae* (MRN complex in humans; (Abraham, 2001; Nakada *et al.*, 2003, 2004; Falck *et al.*, 2005; Cuadrado *et al.*, 2006; Jazayeri *et al.*, 2006). After DNA damage, Mec1 and Tel1 (ATM and ATR in human) cause hyperphosphorylation of Rad9 and the checkpoint kinases, including Chk1, Chk2 (Rad53), and Dun1 (Sanchez *et al.*, 1999; Schwartz *et al.*, 2002; Sweeney *et al.*, 2005; Harrison and Haber, 2006), which are essential for checkpoint control. Activation of checkpoint kinases phosphorylates various effector proteins to heal DNA lesions (Branzei and Foiani, 2006; Putnam *et al.*, 2009). Double-strand break (DSB) repair occurs via either of two pathways: 1) the homologous recombination (HR) pathway, in which Rad51 and Rad52 play key roles, and 2) the nonhomologous end-joining (NHEJ) pathway, which has Ku70, Ku80, DNA PKc, ligase IV, and Mre11 as the main molecular players (Finn *et al.*, 2012). HR yields different products, depending on whether cells use Rad51-dependent, error-free gene conversion (GC) or Rad51-independent, mutagenic, single-strand annealing (SSA; Ivanov *et al.*, 1996; Agmon *et al.*, 2009). NHEJ represents the predominant DSB repair pathway in mammalian cells, but in tumor cells, HR-mediated DNA repair pathway is favored over NHEJ (Mao *et al.*, 2009).

During DNA damage, hyperphosphorylated Rad9 is associated with Rad53 through the interaction between the forkhead-associated domain of Rad53 and the hyperphosphorylated residues in Rad9 (Durocher *et al.*, 1999). Rad9 catalyzes the transphosphorylation of Rad53 in an ATP-dependent manner and thereby activates Rad53 kinase activity. Finally, activated Rad53 is dissociated from Rad9 (Gilbert *et al.*, 2001) and enhances the checkpoint signal in the cell. Rad53-dependent phosphorylation of Swi6 causes inactivation of Swi6/Swi4 complex, which eventually inhibits the transcription of *CLN1* and *CLN2* and thus arrests the cell cycle and causes delay in the G1- to S-phase transition (Sidorova and Breeden, 1997). However, whether Rad53 abundance influences its activity has not been explored.

Hence, to understand explicitly any correlation between inefficient DNA damage responses and heat-stressed conditions, we created an isogenic CEN-based *HSP90* overexpression strain that mimics one of the immediate outcomes of temperature stress. Our study demonstrates that elevated levels of Hsp90 confer hypersensitivity toward methyl methanesulfonate (MMS) and ultraviolet (UV) radiation to the same extent as that observed during short exposure (1 h) to heat shock (40°C). We find that higher expression of Hsp90 channels the repair of chromosomal DSB via the Rad51-independent mutagenic SSA repair pathway instead of Rad51-dependent error-free GC. We demonstrate that Hsp90 abundance inhibits Rad51 recruitment to the broken junction of DNA and hence results in a GC-deficient condition. Further study establishes that Hsp90 is involved in the negative regulation of *RAD53* transcription, and at a higher concentration of Hsp90, cells fail to transmit a Rad53-dependent checkpoint signal. As a result, upon DNA damage, up-regulation of Rad51p is inhibited, and *CLN1* and *CLN2* transcription is elevated significantly in G1-arrested cells. We demonstrate that Hsp90 acts as a master regulator in the DNA damage response pathway by controlling the transcription of the major checkpoint kinase and thereby modulates the DNA repair pathway.

RESULTS

Heat shock or *HSP90* overexpression causes hypersensitivity toward MMS and UV radiation

To understand whether heat shock leads to increased sensitivity toward DNA-damaging agents in our working model system, *S. cerevisiae*, we exposed NKY13 cells simultaneously to 40°C and the genotoxic agent MMS or UV radiation as in *Materials and Methods*. Heat-stressed cells treated with 0.03% MMS for 2 h had >50% decreased survivability (Figure 1A). In a similar manner, heat-stressed cells exposed to varying doses of UV radiation had a significant decrease in viability with increase in UV dose (Figure 1B).

When cells are exposed to heat shock, Hsp90 abundance is increased severalfold as one of the immediate responses. To understand whether *HSP90* overexpression itself is responsible for the increased genome instability, we compared the survivability of isogenic wild-type (NKY13) and *HSP90*-overexpressed (NKY14) cells toward MMS and UV radiation. To reduce experimental variability for each assay, we used a freshly transformed centromeric yeast expression vector that constitutively overexpresses *HSP90* under the control of a GPD promoter. Susceptibility to MMS was tested by subjecting growing cells to 0.03% MMS for only 2 h and then returning them to grow in the absence of MMS. We calculated the percentage survivability of *HSP90*-overexpressing cells. The data revealed 60% reduction in the survivability of cells expressing *HSP90* compared with wild-type cells (Figure 1C). However, the sensitivity was not as drastic as in Δ*rad51*. To establish that the hypersensitivity to MMS is specific to *HSP90* overexpression, we used an isogenic strain (NKY38) that harbors a centromeric yeast vector overexpressing an N-terminal mutant of *hsp90* (G170D) from the GPD promoter. The crystal structure of the N-terminal domain of yeast Hsp90 shows that glycine at position 170 occupies a conformationally restricted position (Prodromou *et al.*, 1997), and mutation of glycine to aspartic acid completely destabilizes the structure of Hsp90 and results in complete loss of function at nonpermissive temperature (Nathan and Lindquist, 1995). It was also reported that G170Dhsp90 is nonfunctional when overexpressed even at permissive temperature (Prodromou *et al.*, 2000). We find that the strain overexpressing mutant G170Dhsp90 is not sensitive toward MMS, however, and shows comparable survivability to the strain harboring empty plasmid (Figure 1C). In addition, we analyzed the sensitivity

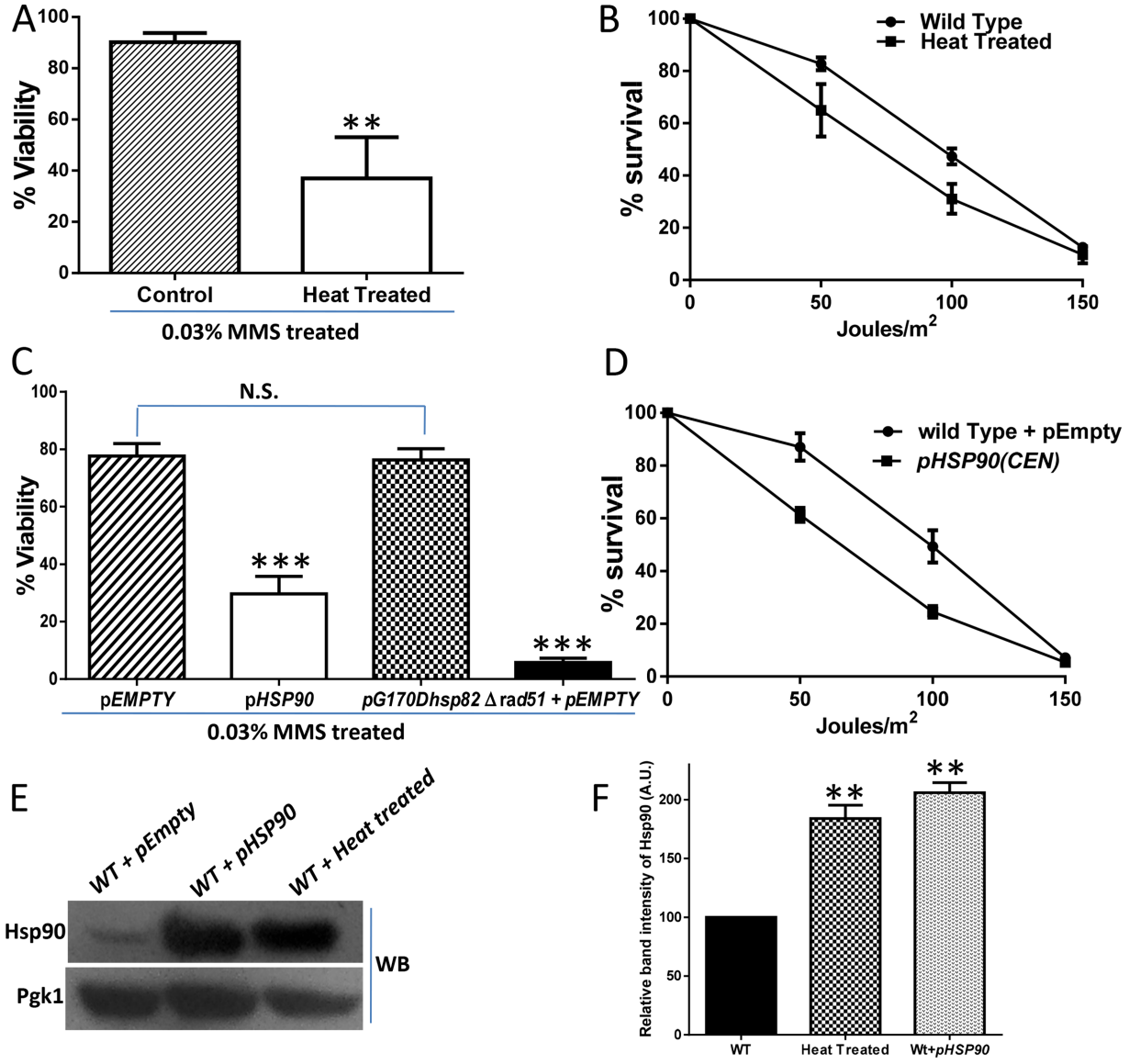

FIGURE 1: Heat shock or *HSP90* overexpression causes hypersensitivity to MMS and UV radiation. (A) Percentage survivability of cells upon treatment with 0.03% MMS for 2 h for wild-type strain (harboring pRS313 empty vector) at normal temperature 30°C and upon heat shock at 40°C. One set of cells (both untreated and treated fractions) was then shifted to 40°C for 1 h and shifted to 30°C for another 1 h of MMS treatment. Equal numbers of cells were then spread on agar plates. Average of three independent experiments ± SD. (B) Percentage survivability to UV radiation for wild-type strain (pRS313 empty vector) at normal temperature 30°C and upon heat shock at 40°C for different UV doses as indicated along the *x*-axis. The cells were grown to mid log phase at 30°C. One set was then shifted to 40°C for 1-h heat shock. Equal numbers of cells were spread on agar plates and immediately exposed to various UV doses. Average of three independent experiments ± SD. (C) Percentage survivability of cells upon treatment with MMS was repeated for *HSP90*-overexpressing strain *pHSP90*, a strain overexpressing *G170Dhsp82* mutant, Δ*rad51* strain, and the isogenic wild-type strain (pEMPTY). Average of five independent experiments ± SD. (D) Percentage survivability to UV radiation for overexpressing *HSP90* strain *pHSP90* (*CEN*) plotted along with its isogenic wild-type strain (harboring pRS313 empty vector) against different UV doses as indicated along the *x*-axis. Average of four independent experiments ± SD. (E) Western blot comparing the increased levels of Hsp90 upon heat shock and through *CEN* plasmid against the wild-type strain. Pgk1 acts as loading control. (F) Quantification of band intensities from three independent batches of cells showing comparable up-regulation of Hsp90 upon heat shock and through overexpression from *CEN* plasmid. **, $p < 0.01$, ***, $p < 0.001$; N.S., not significant.

of *HSP90*-overexpressing cells (NKY14) to increasing doses of UV radiation. Figure 1D shows that UV exposure resulted in a significant drop in the viability of the *HSP90*-overexpressed cells compared with wild type. Our experiment demonstrated that sensitivity to DNA-damaging agents is comparable in heat-stressed cells and cells harboring *HSP90*-overexpression plasmid. Together the results suggest that cells become hypersensitive toward DNA-damaging agents under conditions in which Hsp90 is either naturally or artificially overexpressed. Western blot analysis shows that the level of Hsp90 under heat-stressed conditions (as noted in *Materials and Methods*) is comparable to the amount present in the strain harboring the centromeric *HSP90* overexpression vector (Figure 1E).

Quantitative analysis from three independent batches of cells confirms that the endogenous level of Hsp90 is up-regulated in a comparable manner in both conditions (Figure 1F).

Higher levels of Hsp90 lead to preferential use of SSA over GC and partial loss of NHEJ efficiency

Reduced cell viability of cells with high amounts of Hsp90 points to a probable aberration in either or both of the major DNA repair pathways (namely, NHEJ and HR). To determine the efficiency of HR, we performed a GC assay, which is a specific assay for functional analysis of Rad51. The principle underlying this assay is represented in the schematic diagram in Figure 2A. The wild-type strain NA14 harbors two consecutive *URA3* genes, one of which is inactivated by incorporation of HO endonuclease site within it. The induction of HO by galactose creates a DSB at the mutated *ura3* locus, which uses donor *URA3* situated 3 kb from the HO cut site to repair the break. We sought to determine the repair efficiency and repair choice in wild-type NA14, NA14/*Δrad51*, and the strain carrying the same centromeric *HSP90* overexpression plasmid mentioned earlier (NKY30). Our experimental data established that although there was no significant difference in the repair efficiency among the strains, there was a distinct difference between their repair choices (Figure 2B). Whereas the wild type showed 35% GC efficiency, the *HSP90* overexpression strain used exclusively the Rad51-independent mutagenic SSA pathway, like that of Δ*rad51*. The Western blot in Figure 2B, bottom, shows the overexpression of Hsp90 in the NKY30 strain. This observation raised the question of whether Rad51 recruitment to the damaged sites was affected under such conditions. We used a chromatin immunoprecipitation (ChIP) assay with NA14 and NKY30 strains to observe Rad51 localization to the damaged site. HO endonuclease was expressed in exponentially growing culture, and the DNA sequence close to the donor *URA3* locus was chromatin immunoprecipitated with Rad51 using anti-Rad51 antibody. We observed that the pellet fraction of the wild-type strain was enriched with Rad51 specifically upon HO induction, whereas Rad51 recruitment to the damaged sites was hampered in *HSP90*-overexpressing cells, as evident from the absence of the PCR-amplified band (Figure 2C). To rule out the possibility that the absence of Rad51 in *HSP90*-overexpressing cells was not due to inefficient DNA break upon HO induction, we designed an experiment in which we amplified the HO site flanking *ura3* after 1 h of HO induction. We used a forward primer 20 base pairs upstream of HOcs and a reverse primer (KanB1) complementary to the middle part of the *KANMX* region. We observe the amplified band of the target site under uninduced conditions, in contrast to the disappearance of the amplicon upon HO induction in both wild-type and *HSP90*-overexpressing cells (Figure 2D). To establish that *HSP90* overexpression does not interfere with HO cutting efficiency, we used Δ*rad51* cells, in which HO-induced DNA breaks cannot be repaired by Rad51. We transformed the centromeric *HSP90* overexpression plasmid in Δ*rad51* cells and compared the HO cleavage efficiency between normal and *HSP90*-overexpressing strains in the same manner as described earlier. We found that HO digestion efficiency is comparable between wild-type and *HSP90*-overexpressing strains, as visualized by disappearance of the aforementioned amplicon after 1 h of HO induction in both cell types (Figure 2E). In conclusion, the results clearly suggest that *HSP90* overexpression hampers recruitment of Rad51 at the DSB and as a result uses error-prone SSA instead of error-free GC.

To study the consequence of Hsp90 abundance on the NHEJ mode of repair, we performed an NHEJ-specific assay. The assay uses a strain that harbors two I-SecI sites on either side of the *URA3* gene on chromosome V, as illustrated in Figure 2F. The nuclease (I-SecI)–encoding sequence is placed under a galactose-inducible promoter at a different locus. The haploid nature of the cells does not allow survival upon chromosome breakage by HR. Hence the NHEJ pathway is used by the cells to mend the break. On induction of DSB by galactose, we measured the number of viable cells and total number of cells plated. We observed 50% reduction in NHEJ efficiency when *HSP90* is overexpressed in the cells compared with the cell having an empty plasmid (Figure 2G). The Western blot in Figure 2G, bottom, confirms the overexpression of Hsp90.

Hsp90 causes down-regulation of Rad53 in a dose-dependent manner

The reduction in GC efficiency, as well as in NHEJ, led us to study the steady-state levels of the key proteins involved in these pathways. We used the centromeric *HSP90* overexpression plasmid, and we used Western blotting to compare the steady-state levels of Rad51 and Rad52 in wild-type and *HSP90*-overexpressing cells. We used a Rad52 Myc-tagged strain as wild type and transformed the *HSP90*-overexpressing plasmid in that strain to perform Western blot analysis. Figure 3A shows that the levels of these two proteins did not change with *HSP90* overexpression, which was further confirmed by quantitative analysis using three independent batches of cells, as shown in Figure 3B.

Next we asked whether higher abundance of *HSP90* affects the steady-state levels of the key players in the NHEJ pathway, Ku70 and Ku80. We used a Ku70 and Ku80 Myc-tagged strain. Quantification of the bands using three independent batches of cells revealed no significant change in the levels of Ku70 (Figure 3C); the levels of Ku80, however, were be 1.8- fold up-regulated upon *HSP90* overexpression (Figure 3, D and E). Overall, although we observed a reduction in NHEJ efficiency, the steady-state levels of the proteins required to carry out NHEJ were not reduced.

The lack of any significant changes in the levels of Rad51 and Rad52 led us to examine whether the signaling cascade was affected by *HSP90* overexpression, and so we studied the steady-state levels of the upstream transducer kinases. We performed Western blotting to find any changes in the steady-state levels of the proteins Rad53, Chk1, and Mre11 under wild-type and *HSP90*-overexpressing conditions. Figure 3F shows the Western blots, in which significant reduction of Rad53 is evident in *HSP90*-overexpressing cells. However, no changes are observed in the levels of Chk1 and Mre11 (Figure 3, G and H). The quantification of the band intensities shows approximately twofold reduction in the levels of Rad53 with no notable differences in the levels of Chk1 and Mre11 (Figure 3I). To investigate further whether the observed reduction in Rad53 levels depends on *HSP90* abundance, we studied the levels of Rad53 against a variable *HSP90* overexpression background. To that end, we generated another strain, which harbors a 2μ *HSP90* overexpression plasmid under the control of the GPD promoter. Western blot analysis with proteins isolated from these strains allowed us to compare the levels of Hsp90 and Rad53 among all of these strains (Figure 3J). The quantitative representation of the image from three independent sets of cells confirmed that increase in Hsp90 level leads to sequential decrease in Rad53 level. Whereas the level of Hsp90 increased 6.9 times in a multicopy Hsp90-overexpressing strain compared with wild type, the decrease in Rad53 level was at least 85% compared with wild type and 66% compared with the strain harboring a single-copy Hsp90-overexpressing plasmid (Figure 3K). Thus *HSP90* overexpression specifically reduces the steady-state level of the major checkpoint kinase Rad53 in the cell in a dose-dependent manner.

Hsp90 negatively regulates *RAD53* transcription to suppress the DNA damage response

Next we sought to the find out whether *HSP90* overexpression–mediated down-regulation of Rad53 occurs at the transcript level or at the protein level. Semiquantitative reverse transcription (RT)-PCR showed that the *RAD53* transcript was significantly reduced with *HSP90* overexpression (Figure 4A). We observed a similar reduction in *RAD53* transcript in the heat-induced strain. This shows good correlation between *HSP90*-overexpression and heat-stressed conditions. However, to show specificity toward *HSP90* overexpression, we monitored the level of *RAD53* transcript in NKY38, which overexpresses the *hsp90* mutant. We observed that the *RAD53* transcript remains unaltered like that of the wild type (Figure 4A). Real-time RT-PCR analysis showed >80% reduction in *RAD53* in cells harboring a CEN-based *HSP90* overexpression plasmid compared with wild type (Figure 4B). Overexpression of a protein is often interpreted as the amplification of the normal function of the protein in a cell. We hypothesize that under normal physiological conditions, *HSP90* might act as a negative regulator of *RAD53* transcription. In that case, the *HSP90*-inactivated state would result in an increase in *RAD53* transcription. To test our hypothesis, we monitored the steady-state level of *RAD53* transcript as well as Rad53 protein under the Hsp90-inactivated condition using one of two approaches: using a chemical inhibitor of Hsp90 or a temperature-sensitive mutant of *hsp90*. The function of Hsp90 in the NKY37 strain was inhibited by 40 μM 17-[allylamino]-17-demethoxygeldanamycin (17-AAG). To ensure maximum entry of 17-AAG in the cell, we knocked out the *PDR5* gene, which encodes the export pump (Suhane *et al.*, 2015). Semiquantitative RT-PCR analysis showed that 17-AAG–mediated inhibition of *HSP90* causes derepression of *RAD53* at the transcript level (Figure 4C). Real-time analysis revealed that 17-AAG causes approximately eightfold up-regulation of *RAD53* (Figure 4D). We also isolated the total protein under the 17-AAG–treated condition. Western blot analysis revealed that Rad53 is moderately up-regulated in the Hsp90-inhibitory condition (Figure 4, E and F). As a control, we also analyzed the level of Rad51. Our earlier work showed that 17-AAG treatment causes considerable reduction in the level of Rad51 (Suhane *et al.*, 2015). Similar reduction in Rad51 level (Figure 4E) confirms the 17-AAG–mediated inhibitory condition in the strain. We performed a similar experiment genetically using a *HSP90* nonfunctional mutant. We used the temperature-sensitive strain *iG170Dhsp82*, which behaves like the wild type when grown at a permissive temperature of 25°C and the mutant (y*HSP90*-inactivated state) when grown at a restrictive temperature of 37°C. At 25°C, the strain expresses *HSP90* at normal levels, but at the restrictive temperature (37°C) it behaves like the *HSP90*-inactivated strain. We compared the levels of *RAD53* transcript in *iG170Dhsp82* at 25 and at 37°C. Supplemental Figure S1A clearly shows that *HSP90*-inactivated condition is associated with transcriptional up-regulation of *RAD53*. Real time RT-PCR analysis shows approximately ninefold increase in *RAD53* transcript under the *HSP90*-inactivated condition (Supplemental Figure S1B). Western blot also confirmed that the steady-state levels of Rad53 are up-regulated significantly in the *HSP90*-inactivated condition (Supplemental Figure S1C). To understand the biological significance of such repression, we studied whether a DNA-damaging condition (MMS) would result in the reversal of the transcriptional repression of *RAD53*. We isolated RNA from untreated and MMS-treated wild-type and *HSP90*-overexpressing strains. Real-time RT-PCR showed that 0.03% MMS treatment for 2 h causes approximately twofold increase in the *RAD53* transcript in wild type (Figure 4G). Of interest, *HSP90*-overexpressing cells did not show any significant increase in *RAD53* transcription upon MMS treatment. Real-time RT-PCR data showed that upon MMS treatment, no such up-regulation is visible in *HSP90*-overexpressing cells (isogenic to wild type; Figure 4G). Together our data demonstrate that upon MMS treatment, the steady-state level of *RAD53* in *HSP90*-overexpressing cells remained much lower than that in the wild type. We conclude that the transcriptional repression of *RAD53* under the *HSP90*-overexpressing condition could not be increased by DNA-damaging agents.

Higher abundance of *HSP90* mitigates DNA damage–dependent cell cycle arrest

Given that higher expression of Hsp90 down-regulates the expression of Rad53, we wanted to study whether, under such circumstances, Rad53 is phosphorylated upon DNA damage and whether its reduced amount is sufficient to carry out an efficient checkpoint response. We exposed wild-type and *HSP90*-overexpressing strains to 0.05% MMS for 2 h. The protein was then isolated from untreated and treated fractions in each of the cases and subjected to Western blotting to determine Rad53 phosphorylation status. Figure 5A shows that DNA damage–induced phosphorylation of Rad53 was intact in wild-type and *HSP90*-overexpressing strains, suggesting that upstream kinase function remains intact. Next we monitored whether the lower endogenous level of Rad53 hampers proper functioning of the DNA damage response (DDR) pathway. It was previously established that a Rad53-dependent signal transduction cascade is responsible for transcriptional up-regulation of *RAD51* (Cohen *et al.*, 2002), which subsequently causes an increase in Rad51 level during DNA damage. However, under such conditions, up-regulation of *RAD52* was not found to be drastically different at the transcriptional or translational level (Cohen *et al.*, 2002). We examined the status of Rad51 and Rad52 up-regulation upon DNA damage in wild-type and *HSP90*-overexpressing strains. We exposed cells to two different doses of MMS to monitor the up-regulation of Rad51 (0.05% MMS) and Rad52 (0.15% MMS). The Western blot analysis in Figure 5B showed that in contrast to wild-type cells, in *HSP90*-overexpressing cells, Rad51 was not up-regulated upon MMS treatment. On the other hand, marginal up-regulation of Rad52 upon MMS treatment was observed in both wild-type and *HSP90*-overexpressing cells. Quantitative analysis of blots from three independent experiments showed that in the wild-type strain, there was a 2.5-fold up-regulation of Rad51 upon MMS treatment; however, the DNA damage–induced up-regulation of Rad51 was abrogated under the *HSP90*-overexpressed condition (Figure 5C). A similar effect was also seen when we exposed wild-type and *HSP90*-overexpressing cells to higher doses of UV radiation (3 kJ/m^2). Western blot analysis showed that the up-regulation of Rad51 in UV-treated *HSP90* overexpressed cell was not at par with that observed for the wild-type strain (Figure 5D). Quantitative analysis with three independent experiments revealed that whereas Rad51 up-regulation increased ~2.5-fold in UV-treated wild-type cells, it did not increase significantly in *HSP90*-overexpressing cells (Figure 5E). Changes in the level of Rad52, in accord with the literature, are not so evident in Figure 5, B and D.

It was previously observed that in early-G1-arrested cells, MMS can cause a delay in G1-S transition (Siede *et al.*, 1993, 1994). The MMS-induced delay is characterized by maintenance of low levels of G1 cyclin proteins Cln1 and Cln2, which accumulate slowly, causing resumption of the cell cycle. However, the *rad53* mutant exhibits faster recovery of *CLN1* and *CLN2* compared with the wild type and thus shortens the G1-S delay (Sidorova and Breeden, 1997). We studied whether, upon MMS treatment, *HSP90*-overexpressing cells could cause faster recovery of cyclin kinases in G1 arrest due to lower endogenous levels of Rad53. We studied *CLN1* and *CLN2*

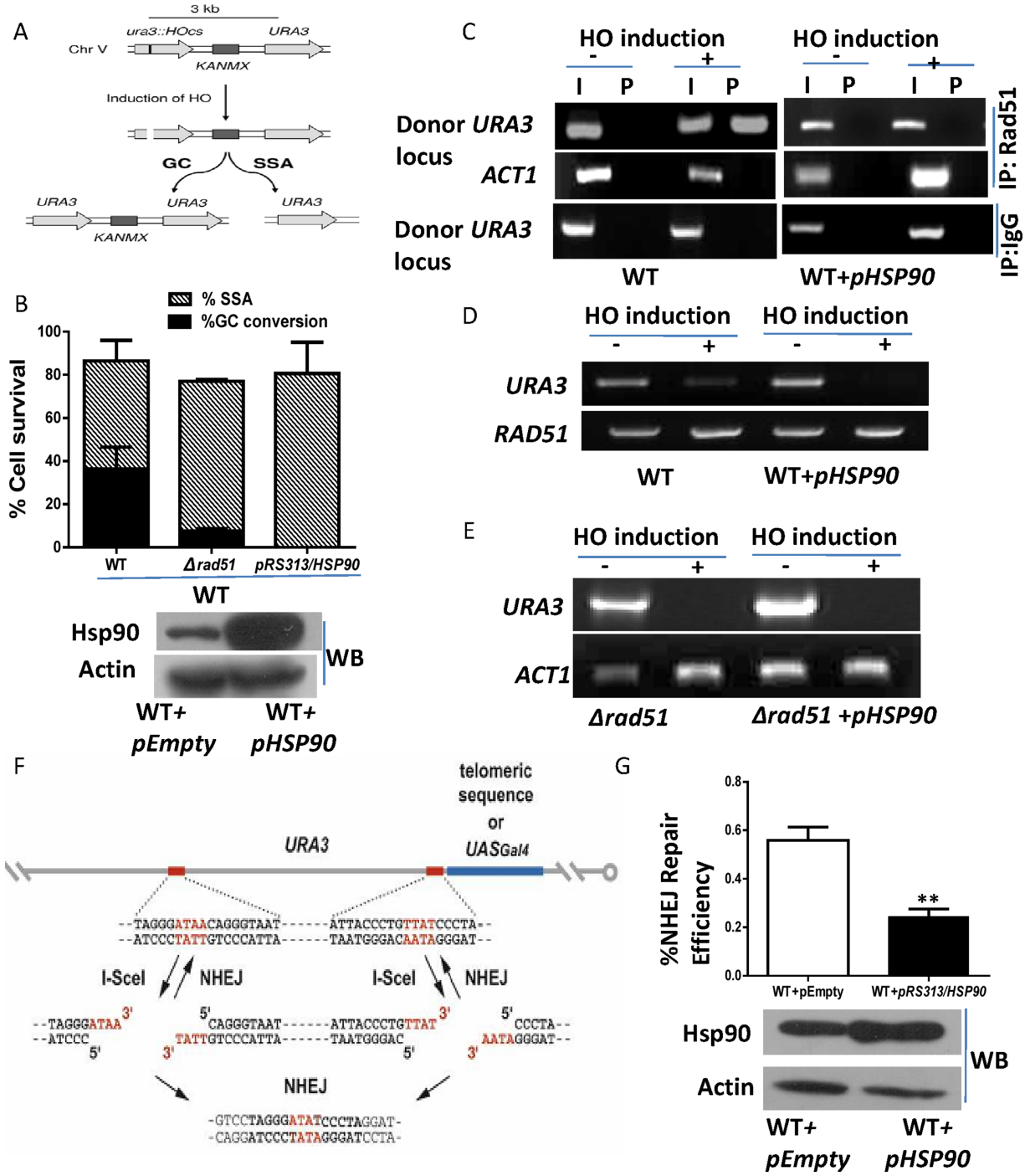

FIGURE 2: Overexpression of *HSP90* leads to preferential use of SSA over GC and partial loss of NHEJ efficiency. (A) The principle behind the GC assay. The cell harbors two copies of the *URA3* gene in a chromosome, one of which is disrupted by incorporation of an HO endonuclease site. The mode of repair taken up by the cell upon HO-induced break gives either of two products: one, which retains the *KANMX* cassette, is repaired by the GC pathway (Rad51 dependent), and one in which the *KANMX* cassette is deleted when repaired by the SSA pathway (Rad51 independent). (B) Percentage of cell survival, with the relevant genotypes marked along the *x*-axis. The filled area represents the fraction of the cells that survived by using the GC mechanism; open bars denote cells that used the SSA mechanism. Bars represent mean value ± SD from three different experiments. Bottom, Western blot confirming *HSP90* overexpression. (C) ChIP assay with wild-type (WT) and *HSP90*-overexpressing (WT + *pHSP90*) strains in the presence (+) and absence (–) of galactose. Anti-Rad51 antibodies were used along with immunoglobulin G (IgG) as control. Input (I) and immunoprecipitated DNA (P) were amplified using primers specific to the Rad51-bound fragment (donor *URA3* fragment) and *ACT1*-specific primers, which act as negative control. (D) Semiquantitative RT-PCR analysis showing the extent of DSB induced with galactose in WT and WT + *pHSP90* (overexpressing *HSP90*) strains. *URA3*-specific region upstream to the HOcs was used as forward primer, and the sequence within the *KANMX* cassette was used as reverse primer. (E) Semiquantitative RT-PCR analysis showing that *HSP90* overexpression does not interfere with HO cutting

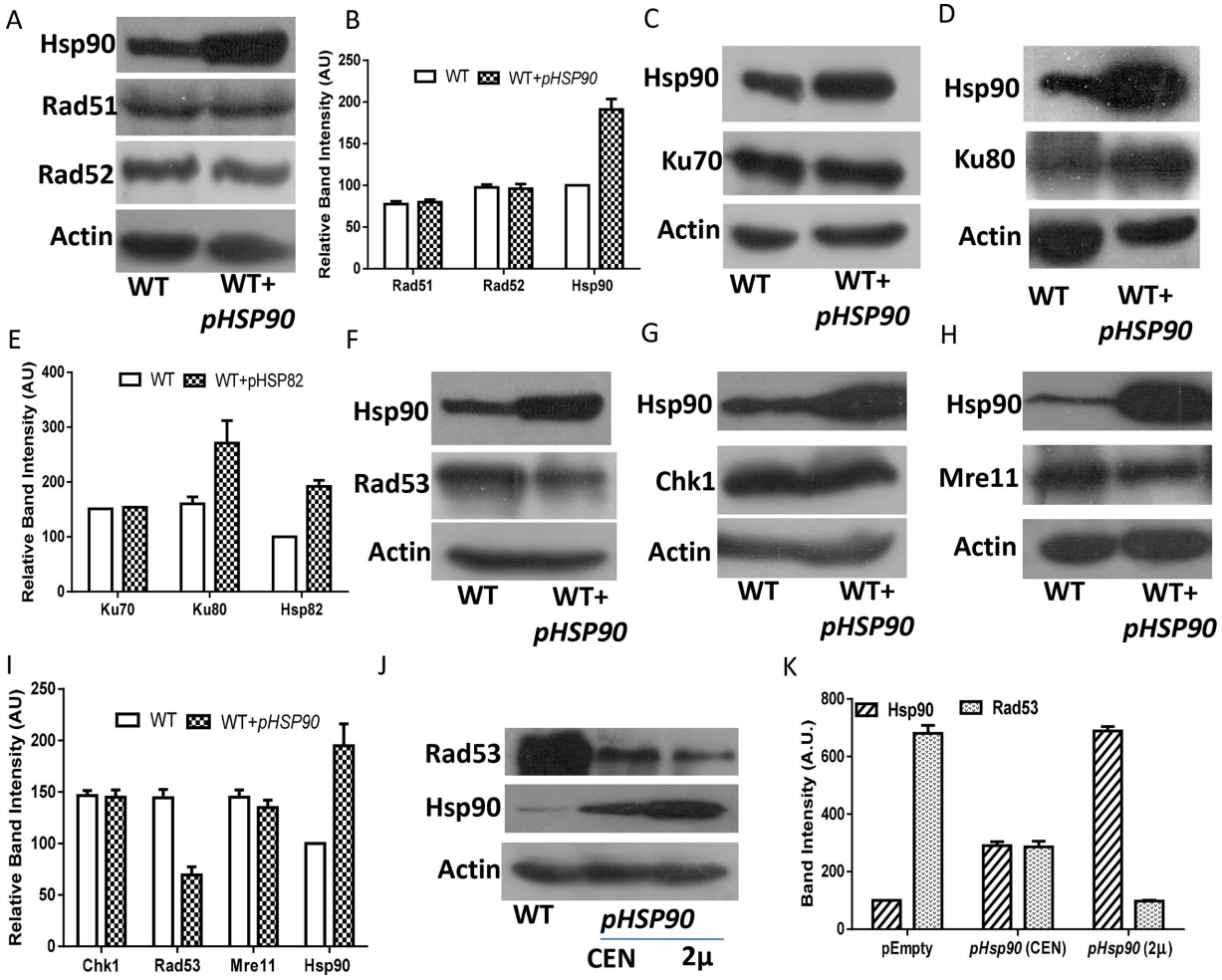

FIGURE 3: Overexpression of *HSP90* causes down-regulation of Rad53 in a dose-dependent manner, (A, C, D, F–H) Western blots showing the steady-state levels of Rad51, Rad52, Ku70, Ku80, Rad53, Chk1, and Mre11 in WT and *HSP90*-overexpressed conditions (WT + *pHSP90*). Actin acts as a loading control. Quantification of the blots showed that (B) Rad51p and Rad52p levels were unchanged with increased *HSP90* level, (E) there was no change in Ku70p, but the level of Ku80 increased with *HSP90* overexpression, and (I) the level of Rad53p decreased, with no significant changes in Chk1p and Mre11p levels, with *HSP90* overexpression. The band intensities in each lane were normalized against actin; mean densities ± SD. (J) Western blot analysis showing Rad53p levels with increasing dose of *HSP90*. CEN represents *HSP90* overexpression by single-copy plasmid, and 2μ represents overexpression by multicopy plasmid. Actin acts as a loading control. (K) Quantification of band intensities showing the sequential reduction in Rad53p level with subsequent increase in *HSP90* level in the cell. Mean densities from two independent blots ± SD.

mRNA levels in wild-type and *HSP90*-overexpressing cells upon DNA damage in G1-arrested cells. The cells were synchronized with α-factor and exposed to 0.2% MMS for 30 min; MMS was subsequently washed, and cells were allowed to grow for another 120 min. RNA was isolated from two fractions—one immediately after MMS exposure and the other after 120 min of growth. Real-time analysis of changes at the transcript level of *CLN1* and *CLN2* (Figure 5F) showed that *CLN1* mRNA reaccumulated faster in *HSP90*-overexpressing cells, and the amount was fivefold higher than in the wild-type strain. Similarly, *CLN2* mRNA levels were 2.5-fold higher in the *HSP90*-overexpressing condition than in the wild type 120 min after MMS treatment (Figure 5G), implying faster reaccumulation in this case as well. These observations suggests that on MMS treatment, Rad53-dependent inhibition of *CLN*s transcription is reversed in *HSP90*-overexpressing cells, which accords well with the reduced activity of Rad53.

It was previously observed that *Δrad53* cells exhibit a slow-growth phenotype (Zhao *et al.*, 1998). In a typical colony growth

efficiency, as shown by the disappearance of *URA3* amplicons in Δ*rad51* and Δ*rad51* + *pHSP90* strains upon galactose induction. (F) Strategy behind the NHEJ assay. *URA3* gene is flanked by two I-SceI sites, where the break is induced upon galactose induction. The measure of the DNA break repair by NHEJ is then evaluated based on the number of colonies grown on galactose-containing medium. (G) Percentage NHEJ efficiency for the strain overexpressing *HSP90* (*HSP90* + *pRS313/HSP90*) and wild-type strain harboring *pRS313* empty vector (WT + *pEMPTY*). Average of three independent experiments ± SD. The *p* value was calculated as 0.0067 using the two-tailed Student's *t* test. Bottom, Western blot confirming overexpression of *HSP90* vs. wild type. $^{**}p < 0.01$.

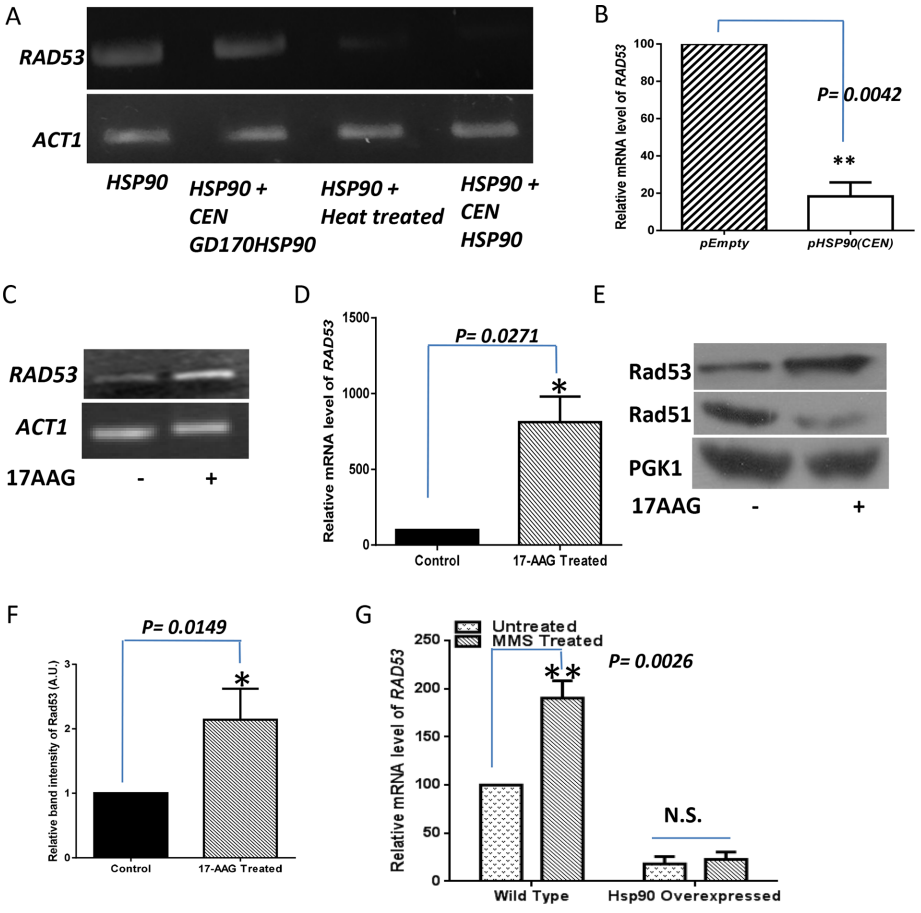

FIGURE 4: Hsp90 negatively regulates *RAD53* transcription to suppress the DNA damage response. (A) Semiquantitative RT-PCR showing the level of *RAD53* transcript in WT (*HSP90*), *G170Dhsp90*-overexpressing (*HSP90 + CEN-GD170HSP90*), heat-induced (*HSP90 + heat treated*), and *HSP90*-overexpressing (*HSP90 +CEN pHSP90*) strains. *ACT1* acts as normalizing control. (B) Real time RT-PCR analysis showing that the relative abundance of *RAD53* mRNA was reduced by 80% in the *HSP90*-overexpressed condition (*pHSP90*). The *p* value was calculated as 0.0042 using the two-tailed Student's *t* test. (C) Semiquantitative RT-PCR showing the level of *RAD53* transcript in absence and presence of 17-AAG (*HSP90*- inhibited condition). (D) Relative abundance of *RAD53* transcript level by real-time RT-PCR revealing significant derepression of *RAD53* in the *HSP90*-inhibitory condition (+17-AAG) vs. the WT condition (–17AAG). The *p* value was calculated as 0.0271 using the two-tailed Student's *t* test. (E) Western blot showing the elevated levels of Rad53p when cells were treated overnight in the presence of 17-AAG. PGK1p acts as loading control and Rad51p as a positive control, whose level is significantly decreased in the presence of 17-AAG, as reported earlier. (F) Quantification of band intensities showing approximately twofold up-regulation of Rad53p upon 17-AAG treatment. The *p* value was calculated as 0.0149 using the two-tailed Student's *t* test. (G) Real-time RT-PCR analysis showing the fold up-regulation of *RAD53* upon 0.03% MMS treatment for 2 h. For WT cells, twofold up-regulation was observed. The *p* value was calculated as 0.0026 using the two-tailed Student's *t* test. However, no significant up-regulation of *RAD53* was observed in the 17-AAG–treated sample. Relative mRNA abundance of *RAD53* was obtained in the *HSP90*-overexpressed strain upon treatment with 0.03% MMS for 2 h. The graph shows that *RAD53* fails to up-regulate upon DNA damage in the *HSP90*-overexpressing condition. *, $p < 0.05$, **, $p < 0.01$; N.S., not significant.

assay, *Δrad53* colonies are 66% smaller than those of the wild type due to presence of excess histone protein in cells (Gunjan and Verreault, 2003). We grew the cells to early log phase and observed them under the microscope. In relation to our previous observations on reduced Rad53 levels in *HSP90*-overexpressing cells, we found that the cells were smaller than the wild-type strain harboring an empty plasmid. The images of cells by confocal microscopy clearly indicated differences in cell size between the strains (Figure 5H). *HSP90*-overexpressing cells were significantly smaller (25%) than the wild type (Figure 5I). Taking the results together, we conclude that in the *HSP90*-overexpressing condition, although damage-induced Rad53 phosphorylation is intact, the lower abundance of Rad53 is unable to mediate an effective checkpoint response, and, as a result, cells behave like the *rad53* mutant.

Overexpression of *RAD53* reverses the DNA damage hypersensitivity conferred by higher levels of Hsp90

To prove that the observations made earlier were indeed due to the reduced level of Rad53, we overexpressed *RAD53* against the *HSP90*-overexpressed background and examined whether the phenotype was reversed. A plasmid carrying *RAD53* fused with *Flag* epitope (*pESC-HIS*) was cotransformed with *HSP90*-overexpression plasmid (*pTA*) in wild-type cells. As a control, empty *pTA* and empty *pESC-HIS* vectors were transformed into the wild-type cells. We also transformed empty *pESC-HIS* and *pTA/HSP90* into the wild-type strain to mimic *HSP90* overexpression in an isogenic background. We performed a DNA damage sensitivity assay using MMS and UV radiation as described previously. The MMS sensitivity assay revealed that overexpression of *RAD53* against the *HSP90*-overexpression background made the cell behave like wild type, as it displayed 76% survival, whereas *HSP90*-overexpressing cells showed only 37% survival (Figure 6A). Similar observations were made upon UV damage (Figure 6B). As a control, we generated only a *RAD53*-overexpressing strain by transforming *pESC-HIS/RAD53* in wild-type cells and performed a DNA damage sensitivity assay. This strain behaved similarly to the wild-type strain, not giving any survival advantage upon *RAD53* overexpression (Figure 6, A and B).

Next we examined whether DNA damage–induced Rad51 up-regulation is restored with *RAD53* overexpression in the *HSP90* overexpressed background. We isolated proteins from untreated and treated fractions of wild-type, *HSP90*-overexpressing, and test strains and performed Western blot analysis. *RAD53* overexpression in the *HSP90*-overexpressing strain restored the Rad51 level comparable to that of wild type upon DNA damage (Figure 6C). MMS treatment caused 2.4-fold up-regulation of Rad51 in the test strain, which is similar to the 2.9-fold up-regulation observed in the wild-type strain (Figure 6D).

Next we studied the levels of *CLN* mRNA in MMS-treated, G1-arrested cells as described previously. We found that test strain prevented premature accumulation of *CLN1* (Figure 6E) and *CLN2* mRNA (Figure 6F), similar to the wild-type strain. The data imply that overexpression of *RAD53* in *HSP90*-overexpressing cells rescues the checkpoint arrest in MMS-treated G1 cells.

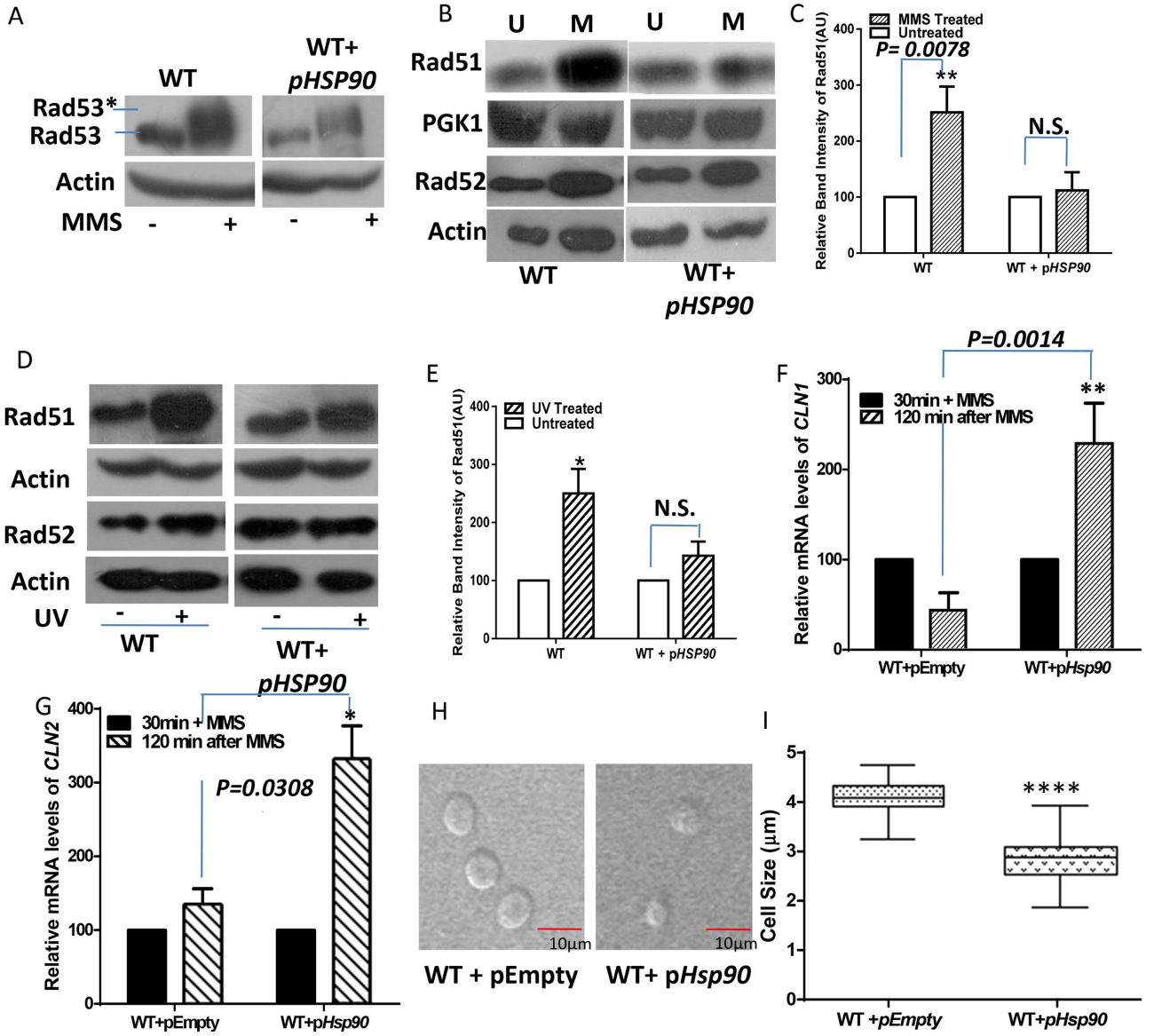

FIGURE 5: Higher abundance of *HSP90* mitigates DNA damage–dependent cell cycle arrest. (A) Western blots showing the status of Rad53p phosphorylation in WT and *HSP90*-overexpressing (WT + *pHSP90*) strains upon treatment with DNA-damaging agent. The blot represents the protein isolated from both strains before and after treatment with 0.05% MMS for 2 h. The Rad53-phosphorylated form is marked as Rad53*. Actin acts a loading control. (B) Western blot analysis showed up-regulation of Rad51p in WT, but no such up-regulation was observed in WT + *pHSP90* strain upon 0.05% MMS treatment (M); also shown are levels of Rad52p in untreated (U) and 0.15% MMS-treated (M) samples in these strains. PGK1 and actin acts as loading controls for monitoring Rad51p and Rad52p levels, respectively. (C) Quantification of band intensities from three independent experiments displayed 2.5-fold up-regulation for Rad51p in the wild-type condition upon MMS treatment, but no such up-regulation is evident in the *HSP90*-overexpressing strain. The band intensities in each lane are normalized against PGK1, and mean densities ± SD are plotted. (D) Western blot analysis showing up-regulation of Rad51p and Rad52p in WT and WT + *pHSP90* strains from untreated (–) and treated (+) fractions with 3-kJ/m^2 dose of UV radiation followed by growth for 3 h. Actin acts as loading control. (E) Quantification of band intensity from three independent experiments normalized against actin. Mean densities ± SD reveal minimal up-regulation of Rad51p in the *HSP90*-overexpressing strain. (F, G) Real-time RT-PCR shows relative abundance of *CLN1* and *CLN2* transcripts, respectively, for WT (WT + *pEMPTY*) and *HSP90*-overexpressing strains. The reaccumulation status of both the transcripts was studied by comparing the mRNA levels from one fraction exposed to 0.2% MMS for 30 min (30 min + MMS) with a fraction in which the cells were allowed to grow for 120 min after MMS treatment in fresh medium. (H) Microscopic images showing the relative cell sizes for WT (WT + *pEMPTY*) and *HSP90*-overexpressing cells. The experiment was performed twice with >100 cells. Representative images. (I) Different cell sizes observed for the strains, showing that the average cell size for the *HSP90*-overexpressing strain was significantly smaller than that of the wild-type strain. The *p* value was calculated as <0.0001 using the two-tailed Student's *t* test. *, $p < 0.05$, **, $p < 0.01$, ****, $p < 0.0001$; N.S., not significant.

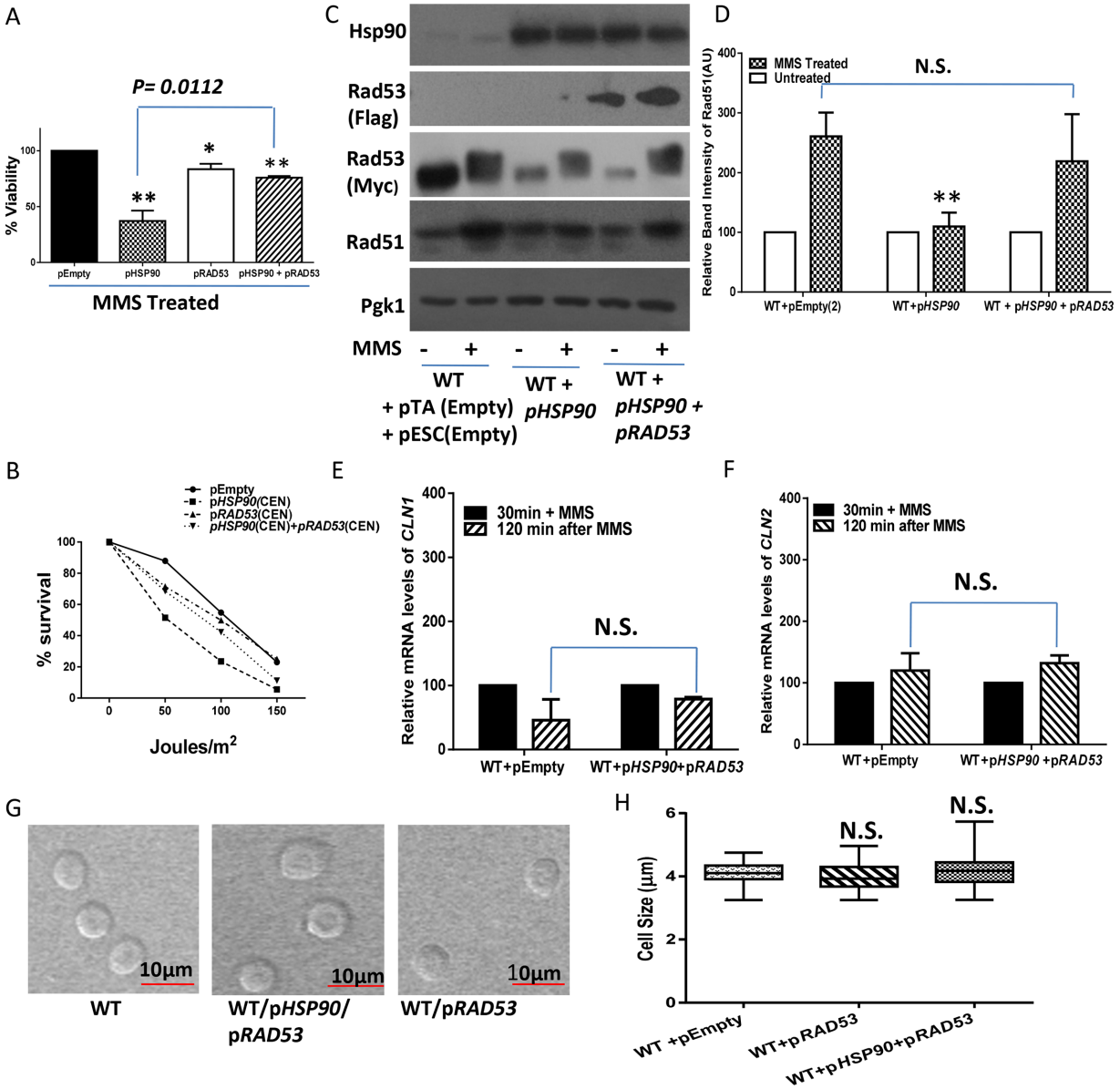

FIGURE 6: Overexpression of *RAD53* in *HSP90*-overexpressing cell restores DNA damage hypersensitivity. (A) Percentage survivability of four different strains upon 0.03% MMS treatment plotted as indicated along the *x*-axis. Average viability ± SD for each strain from five independent experiments. (B) Percentage survivability to UV radiation for the same sets of strains as in A against different UV doses as indicated along the *x*-axis. (C) Representative Western blots, showing the restoration of Rad51p up-regulation upon treatment with MMS in the WT + p*HSP90* + p*RAD53* strain compared with the *HSP90*-overexpressing strain. The increased level of Rad53p in the *RAD53*-overexpressing strain is shown by probing with anti-Flag antibody. –, MMS-untreated fraction; +, fractions treated with 0.05% MMS for 2 h. Pgk1 acts as loading control. Rad53p level was monitored using anti-Flag antibody. (D) Quantification of band intensities from two independent experiments showing that the extent of up-regulation of Rad51p in the wild-type strain (WT + pEMPTY(2)) is similar to that for the WT + p*HSP90* + p*RAD53* strain. Each lane was normalized against actin. Average band intensities ± SD. (E, F) Real time RT-PCR showing relative abundance of *CLN1* and *CLN2* transcripts, respectively, for the strains noted along the *x*-axis. There was no significant change between the levels of G1-cyclins from the 30-min, MMS-treated samples in G1-arrested cells and the 120-min post–MMS treatment samples. (G) Representative cell images for WT, the strain overexpressing *RAD53* against the *HSP90*-overexpression background (WT + p*HSP90* + p*RAD53*), and the *RAD53*-overexpressing (WT + p*RAD53*) strain. (H) Average cell size (*y*-axis) for each strain type (*x*-axis). Sample size > 100. Cell sizes all lie in the same range. Error bar indicates ±SD. *, $p < 0.05$, **, $p < 0.01$; N.S., not significant.

We also studied whether the smaller cell size attributed to *HSP90* overexpression was due to the reduction of Rad53 levels. We compared the cell size in the three strains (Figure 6G) and found no significant differences in diameter (Figure 6H).

DISCUSSION

Hyperthermia is a promising treatment to arrest cancer growth and is used along with radiation therapy. Treatment with hyperthermia is under clinical trial, but the mechanism behind it is poorly

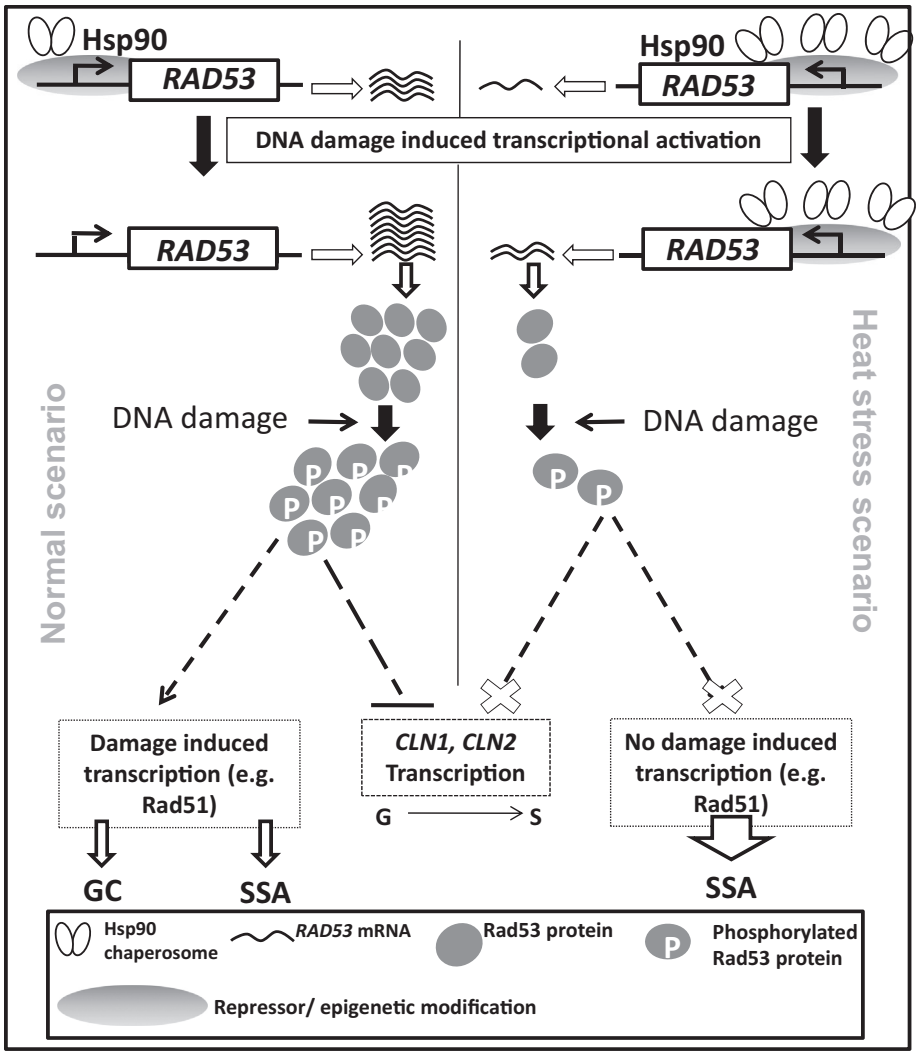

FIGURE 7: Model of the regulatory role of Hsp90 in the DNA damage response. Hsp90 keeps the transcription of *RAD53* in a repressed state under normal condition. On DNA damage, this repression is removed, and *RAD53* transcription is up-regulated. Upstream kinases then phosphorylate Rad53p. The activated/phosphorylated form of Rad53p thereby performs its downstream functions, which aid in cell survival. However, overexpression of *HSP90* increases the extent of repression of *RAD53* transcription in the normal state. Therefore the extent of up-regulation of *RAD53* upon DNA damage under such conditions is not on a par with the normal wild-type condition. As a result, there is less of the activated form of Rad53p synthesized in the cell, which is the cause of the abrogation of its downstream functions. Thus mutagenic SSA repair is used.

understood. Hyperthermia induces the expression of heat-shock proteins, but whether this has deleterious effects on DNA damage response pathways has not been studied. Here, we established an important link between Hsp90 abundance—a spontaneous outcome of hyperthermia—and DNA damage sensitivity. We found that the model eukaryotic organism *S. cerevisiae* displays marked sensitivity toward MMS and UV radiation when exposed to high temperature (40° C for 1 h). Hyperthermia is associated with changes in global expression of proteins. To decipher whether the observed phenotype is the immediate outcome of Hsp90 overexpression, we designed our experimental system in isogenic yeast strains in which similar levels of overproduction of Hsp90 were maintained across different experiments by using a single-copy, CEN-based *HSP90* expression vector. Our study reveals that increased expression of Hsp90 is associated with fivefold reduction in *RAD53* transcript, resulting in a considerable reduction in the steady-state level of Rad53. This leads to poor DNA damage response and inaccurate DSB repair. Our results show that increased expression of Hsp90 also inhibits DNA damage–induced up-regulation of Rad53, and thus its abundance does not reach the wild-type level. We hypothesize that to trigger an effective DNA damage response, a threshold amount of Rad53 is essential. On the basis of the following lines of evidence, we conclude that lower abundance of Rad53 is unable to manifest optimum DNA damage response and hence leads to improper DNA repair. First, DNA damage–induced up-regulation and recruitment of Rad51p at the DSB sites are absent, leading to a complete loss of GC. Second, NHEJ is also partially inhibited. Third, there is premature accumulation of *CLN1* and *CLN2* in MMS-induced, G1-arrested cells. Finally, the average cell size is significantly smaller than the wild type, a phenotype associated with checkpoint defects. Our conclusion that the observed phenotypes stem from down-regulation of *RAD53* due to higher abundance of Hsp90 is further supported by the fact that overexpression of *RAD53* in the *HSP90*-overexpression background reverses DNA damage hypersensitivity and restores an effective DNA damage response pathway.

Taking the results together, we propose the following model. The transcriptional repression of *RAD53* by Hsp90 seems to be economical for the cell, as it aids in complete shutdown of the signaling cascade in the absence of DNA damage, which allows the cell to enter into the cell cycle. In response to DNA damage, Rad53 is phosphorylated as well as up-regulated significantly. If the level of Hsp90 is high in the cell, Rad53 phosphorylation is not affected per se, which indicates that Rad9 function remains intact. However, due to the reduced steady-state level of Rad53, the effective concentration of phosphorylated Rad53 remains below the threshold level and so it cannot initiate downstream signaling events. As a result, the components of GC machinery are not recruited at the DSB, and cells thus use the mutagenic SSA pathway as the sole repair pathway (Figure 7). It is important to note that under higher expression of Hsp90, creation of a single DSB in DNA does not reduce overall cell survivability because under such conditions, Rad52 up-regulation upon DNA damage is maintained in the cell and thus the Rad52-dependent SSA repair pathway can take over.

So far we have discussed how hyperthermia-induced overexpression of Hsp90 attenuates Rad53-mediated DDR and leads to genomic instability. However, one cannot rule out the possibility that hyperthermia may also result in the denaturation of certain DNA repair proteins and thus lead to genomic instability. On the other hand, it is also possible that hyperthermia-induced heat-shock proteins might actually rescue the damaged/misfolded proteins.

Future research is required to completely understand these complex phenomena.

In *S. cerevisiae*, Rad53 is the major checkpoint kinase, and improper activation of this upstream molecule leads to defects in the downstream effecter pathways, which include both HR and NHEJ. Thus it is not surprising that Hsp90 overexpression affected NHEJ efficiency despite the fact that the steady-state level of yKu80, one of the major proteins in this pathway, was increased. It is also possible that other components of the NHEJ machinery could be affected directly or indirectly, or there may be a defect in their recruitment to the broken DNA junction. These possibilities are worth pursuing but are outside the scope of this article. It is important to note that the human system is different from that of yeast with respect to the use of repair pathways. As opposed to yeast, which predominantly use HR, under normal conditions, human cells preferably use the NHEJ pathway. However, it has been reported that tumor cells preferably use HR over NHEJ (Mao *et al.*, 2009). Thus it will be interesting to explore whether Hsp90 overexpression causes similar defects in the HR pathway in tumor cells.

A higher abundance of Hsp90 is beneficial for cancer cell survival and maintenance, as it chaperones many oncogenic proteins. Our study provides compelling evidence in favor of a hypothesis that poorer DNA damage repair efficiency in cancer cells is correlated with higher abundance of Hsp90, as our results show a direct link between Hsp90 abundance and inefficient activation of the DNA damage response pathway. This is of special interest because tumors have varying expression levels of heat-shock proteins, and heat-shock components are being explored as therapeutic targets for cancer. It was reported that the mammalian orthologue of Rad53, Chk2, is transcriptionally down-regulated in a p53-dependent manner through the action of the transcription factor NF-Y (Matsui *et al.*, 2004). Given that p53 is a direct client of Hsp90 (Walerych *et al.*, 2004), it will be interesting to investigate how Hsp90 homeostasis modulates *CHK2* transcription.

It is not clear how the presence of a genotoxic agent induces *RAD53* transcription, although the Hsp90 level is altered during the DNA damage response. One speculation is that in the presence of genotoxic stressors, Hsp90 proteins are redistributed in the cells, and many DNA repair proteins require Hsp90 activity. Alternatively, it may be possible that in the presence of DNA-damaging agents, the transcriptional repression mediated by Hsp90 is lifted. In *Drosophila*, Hsp90 negatively regulates the transcription of several environmentally regulated genes, as well as signal transducer genes, by stabilizing RNA polymerase II pause by interacting with the negative elongation factor (NELF; Sawarkar *et al.*, 2012). In *S. cerevisiae*, an orthologue of NELF is absent. Thus future study is required to unravel the mechanism behind such transcriptional regulation.

MATERIALS AND METHODS

Plasmids

Sequences of all of the primers used in this study are given in Table 1. To mimic *HSP90* overexpression in cells, the centromeric plasmid *pRS313/yHSP90* (Laskar *et al.*, 2011) and the 2 μ plasmid *pBEVYT/yHSP90* (Laskar *et al.*, 2011) were used. To overexpress the mutant form of yHsp90, single-copy centromeric plasmid piHGpd/G170D was purchased from Addgene (Cambridge, MA). This plasmid harbors y*HSP90*, with a glycine-to–aspartic acid mutation at amino acid 170. The expression of the mutant gene is regulated by the strong constitutive promoter GPD (Nathan and Lindquist,1995). The C-terminal *MYC* tagging of the strains at the chromosomal locus and the targeted gene knockouts were performed using pFA6a-13myc-*KANMX/TRP/HIS* and pFA6a-*KANMX/TRP/HIS* plasmids, respectively (Longtine *et al.*, 1998). Using W303α genomic DNA as a template, we amplified full-length *RAD53* using the primer pairs OSB 263 and OSB 264 and successfully cloned in in the 2μ C-terminal Flag-tagged vector *pESC-HIS* (Agilent Technologies, Santa Clara, CA). The recombinant vector *pESC-RAD53-flag* thus generated overexpresses *RAD53* under the *GAL* promoter.

Yeast strains

Strains used in this study are listed in Table 2. For DNA damage sensitivity studies, W303α, MKB201, NA14, and LS402 strains were individually transformed with centromeric *pRS313/HSP90* to generate NKY14, NKY6, NKY30, and NKY36 strains, respectively. Similarly, centromeric piHGpd/G170D plasmid was transformed into W303α to generate NKY38. Empty pRS313 vector was transformed in W303α and LS402 to generate NKY13 and NKY35, respectively. An array of 13myc-tagged strains was generated for tagging of *RAD53*, *CHK1*, *RAD52*, *MRE11*, and *KU80* from W303α to generate NKY15, NKY17, SLY47, MVS20, and MVS23, respectively, using the primer pairs OSB 81–82, OSB 97–98, OSB 68–69, OMKB 179–180, and OMKB 181–182 respectively. The *HSP90* overexpression plasmid *pRS313/HSP90* was transformed into NKY15, NKY17, SLY47, MVS20, and MVS23 strains, and colonies were selected on synthetic complete –His medium to generate isogenic strains NKY16, NKY18, NKY20, NKY25, and NKY26, respectively.

The plasmid *pESC-RAD53-MYC* was transformed into W303α to generate NKY23. The experiments pertaining to rescue of the DNA damage–sensitive phenotype were performed with strains NKY28, which harbors empty *pBEVYT* and empty *pESC* vectors; NKY29, with *pBEVYT/HSP82* and empty *pESC* vector; and NKY24, harboring *pBEVYT/HSP82* and *pESC/RAD53* vectors.

MMS and UV sensitivity assays

Sensitivity to DNA-damaging agent was determined in the presence of MMS by growing fresh yeast cells in selective medium at 30°C to OD 0.5, which was then divided into two portions of equal volume. One portion of the cells was exposed to 0.03% (vol/vol) MMS (Sigma-Aldrich, St. Louis, MO) for 2 h, and the other batch was exposed to 40°C coupled to 0.03% (vol/vol) MMS for 1 h and then returned to 30°C with continued MMS exposure for an additional 1 h such that MMS exposure was restricted to 2 h. After that, MMS was washed out from heat-treated and untreated cells, and 1000 cells were plated from each batch and incubated at 30°C. The plates were incubated for 36 h, and their growth was compared. The ratio of the number of cells grown in the absence of MMS to the cells grown in the presence of MMS was multiplied by 100, which gave the percentage survival. Each assay was repeated at least three or four times. In a similar manner, cells having empty vector and Hsp90 expression vector were treated with same concentration of MMS for 2 h, and percentage survivability was calculated.

For the UV sensitivity assay, the cells were grown in selective medium to log phase. One portion of the cells was exposed to 40°C for 1 h, and the other batch was incubated at 30°C for 1 h. After that, 1000 cells were estimated and plated to determine the number of viable colony-forming units for each indicated dose of UV radiation in Joules/square meter. The required intensity of UV irradiation was achieved out using a Stratagene Stratalinker 1800. The plates were incubated for 4 d, the number of viable colonies for each indicated dose of UV radiation was counted, and the percentage survivability was calculated.

Primer	Sequence	Purpose
OSB 263	5′ ACT GAA TTC ATG GAA AAT ATT ACA CAA CCC AC 3′	Forward primer used to amplify Rad53 for cloning in *pESC-MYC* tagged vector
OSB 264	5′ ACG ATC GAT CGA AAA TTG CAA ATT CTC GGG 3′	Reverse primer used to amplify Rad53 for cloning in *pESC-MYC* tagged vector
OSB 81	5′ GGA CCA AAC CTC AAA AGG CCC CGA GAA TTT GCA ATT TTC GCG GAT CCC CGG GTT AAT TAA 3′	Forward primer used to generate *MYC* tag at the C-terminal end of *RAD53* at the chromosomal locus
OSB 82	5′ TTA AAA AGG GGC AGC ATT TTC TAT GGG TAT TTG TCC TTG GGA ATT CGA GCT CGT TTC AAC 3′	Reverse primer used to generate *MYC* tag at the C-terminal end of *RAD53* at the chromosomal locus
OSB 97	5′ AAT TTC AAC TAT CTG TAG GGA TAT TAT CCT AAT TCC CAA CCG GAT CCC CGG GTT AAT TAA 3′	Forward primer used to generate *MYC* tag at the C-terminal end of *CHK1* at the chromosomal locus
OSB 98	5′ TGA TCA GTG CAT CTT AAC CCT TCT TTT GTC TCC ATT TTT TGA ATT CGA GCT CGT TT AAA C 3′	Reverse primer used to generate *MYC* tag at the C-terminal end of *CHK1* at the chromosomal locus
OSB 68	5′ AAG ACC AAA GAT CAA TCC CCT GCA TGC ACG CAA GCC TAC TCG GAT CCC CGG GTT AAT TAA 3′	Forward primer used to generate *MYC* tag at the C-terminal end of *Rad52* at the chromosomal locus
OSB 69	5′ ATA ATG ATG CAA ATT TTT TAT TTG TTT CGG CCA GGA AGC GGA ATT CGA GCT CGT TTA AAC 3′	Reverse primer used to generate *MYC* tag at the C-terminal end of *RAD52* at the chromosomal locus
OMKB 179	5′ GAC GGA TAT TCT TGG AAG TCT CCT TGC TAA GAA AAG AAA AGG GAT CCC CGG GTT ATT AA 3′	Forward primer used to generate *MYC* tag at the C-terminal end of *ScMRE11* at the chromosomal locus
OMKB 180	5′ TTA TAA ATA GGA TAT AAT ATA ATA TAG GGA TCA AGT ACA AGA ATT CGA GCT CGT TTA AAC 3′	Reverse primer used to generate *MYC* tag at the C-terminal end of *ScMRE11* at the chromosomal locus
OMKB 181	5′ TGA ACA ACA CAG TAG GGG AAG TCC AAA CAA TAG CAA TAA TGG GAT CCC CGG GTT AAT TAA 3′	Forward primer used to generate *MYC* tag at the C-terminal end of *ScKu80* at the chromosomal locus
OMKB 182	5′ GTG GTG ACG AAA ACA TAA CTC AAA GGA TGT TAG ACC TTT TGA ATT CGA GCT CGT TTA AAC 3′	Reverse primer used to generate *MYC* tag at the C-terminal end of *ScKu80* at the chromosomal locus
OSB 16	5′ TGA CCA AAC TAC TTA CAA CTC C 3′	Forward primer used to amplify *ACT1* for real-time RT-PCR
OSB 14	5′ TTA GAA ACA CTT GTG GTG AAC G 3′	Reverse primer used to amplify *ACT1* for real-time RT-PCR
OSB 244	5′ ACC ATT CAT CGC CGA TCA CC 3′	Forward primer used to amplify *CLN1* for real-time RT-PCR
OSB 245	5′ TCA CAG TTG AGA GCT ATT GTG 3′	Reverse primer used to amplify *CLN1* for real-time RT-PCR
OSB 246	5′ GTG GTA GCA CCG TTA GTG TG 3′	Forward primer used to amplify *CLN2* for real-time RT-PCR
OSB 247	5′ CTA TAT TAC TTG GGT ATT GCC C 3′	Reverse primer used to amplify *CLN2* for real-time RT-PCR
OSB 230	5′ CAG ATG ATG GCA GCT CAA CG 3′	Forward primer used to amplify *RAD53* real-time RT-PCR
OSB 231	5′ GGG TAT TTG TCC TTG GTT ACG 3′	Reverse primer used to amplify *RAD53* real-time RT-PCR
OSB 278	5′CAT GCA AGG GCT CCC TAG C 3′	Forward primer used to amplify *URA3* region for ChIP
OSB 279	5′ CAA CCA ATC GTA ACC TTC ATC T 3′	Reverse primer used to amplify *URA3* region for ChIP
OSB 289	5′ GTT AGT TGA AGC ATT AGG TCC 3′	Forward primer used to confirm HO digestion
KanB1	5′ TGT ACG GGC GAC AGT CAC AT 3′	Reverse primer used to confirm HO digestion
OMKB 90	5′ GGA TCC TGT CTC AAG TTC AAG AAC 3′	Forward primer used to amplify full length *RAD51*
OMKB88	5′ CTG CAG CTA CTC GTC TTC TTC TC 3′	Reverse primer used to amplify full length *RAD51*

TABLE 1: Primers used in this study.

NHEJ assay

MKB201 and NKY6 were freshly streaked on 2% glucose–containing synthetic medium lacking uracil at 30°C for 24 h. At an appropriate dilution, equal numbers of cells were divided into two groups. One group was plated onto glucose-containing synthetic medium lacking uracil, and the other group was plated onto 3% galactose–containing medium containing uracil. All of the plates were incubated at 30°C for 4 d. The percentage NHEJ efficiency was evaluated by multiplying the ratio of cells grown on galactose-containing plates to that grown on glucose-containing plates by 100 (Marcand *et al.*, 2008).

GC assay

This assay was performed using strain NA14, in which a cassette is integrated into chromosome V, where two consecutive *URA3* genes are separated by *KANMX6* (Agmon *et al.*, 2009). The first mutant version of the *ura3* gene harbors an *HO* endonuclease recognition site. *HO* endonuclease is expressed upon galactose induction by growing the strain on galactose-containing medium. The induction of *HO* creates a DSB at the mutated *ura3* locus for which the repair efficiency and repair choice are determined. To carry out the assay, cells from each of the strains NA14, NA14/*Δrad51*, and NKY30 were allowed to grow on the medium

Strain	Genotype	Source
W303α	*MATα 15ade2-1, ura3-1, 112 his 3-11, trp1, leu2-3*	This study
MKB201	*MATa 15ade2-1, ura3-1, 112 his 3-11, trp1, leu2-3 bar1-Δ lys2::pGAL-ISCEI ISceI::URA3::ISceI*	Marcand *et al.* (2008)
NA14	*MATa -inc ura3-HOcs lys2::ura3-HOcs-i nc ade3:: GALHO ade2-1 leu2-3112 his3-11,15 trp1-1 can1-100*	Agmon *et al.* (2009)
LS402	*MATa leu2-3112 trp1-1, can1-100, ura3-1, his 3-11, ade2-1, RAD51::LEU2*	This study
NKY14	*MATα 15ade2-1, ura3-1, 112 his 3-11, trp1, leu2-3, pRS313/HSP90*	This study
NKY6	*(MATa 15ade2-1, ura3-1, 112 his 3-11, trp1, leu2-3 bar1-Δ lys2::pGAL-ISCEI ISceI::URA3::ISceI) pRS313/HSP82*	This study
NKY30	*MATa -inc ura3-HOcs lys2::ura3-HOcs-i nc ade3:: GALHO ade2-1 leu2-3112 his3-11,15 trp1-1 can1-100, pRS313/HSP90*	This study
NKY36	*MATa leu2-3112 trp1-1, can1-100, ura3-1, his 3-11, ade2-1, RAD51::LEU2, pRS313/HSP90*	This study
NKY38	*MATa leu2-3112 trp1-1, can1-100, ura3-1, his 3-11, ade2-1, RAD51::LEU2, piHGpd/G170D*	This study
NKY37	*MATα 15ade2-1, ura3-1, 112 his 3-11, trp1, leu2-3, RAD53-13MYC::KANMX6, PDR5:: LEU2*	This study
NKY13	*MATα 15ade2-1, ura3-1, 112 his 3-11, trp1, leu2-3, pRS313*	This study
NKY35	*MATa leu2-3112 trp1-1, can1-100, ura3-1, his 3-11, ade2-1, RAD51::LEU2, pRS313*	This study
NKY15	*MATα 15ade2-1, ura3-1, 112 his 3-11, trp1, leu2-3, RAD53-13MYC::KANMX6*	This study
NKY17	*MATα 15ade2-1, ura3-1, 112 his 3-11, trp1, leu2-3, CHK1-13MYC::TRP*	This study
SLY47	*MATα 15ade2-1, ura3-1, 112 his 3-11, trp1, leu2-3, RAD52-13MYC*	This study
MVS20	*MATα 15ade2-1, ura3-1, 112 his 3-11, trp1, leu2-3, MRE11-13MYC::KANMX6*	This study
MVS23	*MATα 15ade2-1, ura3-1, 112 his 3-11, trp1, leu2-3, Ku80-13MYC::KANMX6*	This study
NKY16	*MATα 15ade2-1, ura3-1, 112 his 3-11, trp1, leu2-3, RAD53-13MYC::KANMX6, pRS313/HSP90*	This study
NKY18	*MATα 15ade2-1, ura3-1, 112 his 3-11, trp1, leu2-3, CHK1-13MYC::TRP, pRS313/HSP90*	This study
NKY20	*MATα 15ade2-1, ura3-1, 112 his 3-11, trp1, leu2-3, RAD52-13MYC::KANMX6, pRS313/HSP90*	This study
NKY25	*MATα 15ade2-1, ura3-1, 112 his 3-11, trp1, leu2-3, MRE11-13MYC::KANMX6, pRS313/HSP90*	This study
NKY26	*MATα 15ade2-1, ura3-1, 112 his 3-11, trp1, leu2-3, Ku80-13MYC::KANMX6, pRS313/HSP90*	This study
NKY23	*MATα 15ade2-1, ura3-1, 112 his 3-11, trp1, leu2-3, pESC/RAD53*	This study
NKY28	*MATα 15ade2-1, ura3-1, 112 his 3-11, trp1, leu2-3, pESC, pBEVYT*	This study
NKY29	*MATα 15ade2-1, ura3-1, 112 his 3-11, trp1, leu2-3, pESC, pBEVYT/HSP90*	This study
NKY24	*MATα 15ade2-1, ura3-1, 112 his 3-11, trp1, leu2-3, pESC/RAD53, pBEVYT/HSP90*	This study

TABLE 2: Yeast strains used in this study.

plate containing glycerol as a carbon source. We calculated and plated ~1000 cells on glucose- and galactose-containing plates separately and counted colonies after 3–5 d of incubation at 30°C. The ratio of the number of colonies grown on the medium containing galactose compared with that grown on medium containing glucose (no HO induction) determines repair efficiency. However, the repair of the induced DSB could be achieved by GC or SSA. Hence, to determine the efficiency of repair choice, each colony obtained on galactose-containing plates was patched onto plates containing G418 sulfate. If the repair occurred via SSA, it would lead to elimination of the *KANMX6* cassette, making the cells sensitive to G418 sulfate, whereas the GC mode of repair would retain it. Therefore percentage repair choice was evaluated by comparing the viable patches to the total number of patches on the plate. This assay was performed three times, and the mean value was plotted using GraphPad Prism software.

Real-time RT-PCR

To determine the levels of *CLN1* and *CLN2*, the W303α, NKY14 and NKY24 strains were grown to OD 0.5 and subsequently exposed to 0.2% MMS for 2 h. Immediately after, we extracted the amount of cells corresponding to OD 10. The rest were washed to remove MMS and allowed to grow for another 2 h; after that, cells corresponding to OD 10 were extracted. Total RNA was then isolated from these two batches by the acid phenol method (Laskar *et al.*, 2011), and cDNA was synthesized using reverse transcriptase (Omni Script; Qiagen, Hilden, Germany). In a similar manner, cDNA was made from W303α, NKY38, NKY14, and heat-treated W303α strains to study the steady-state levels of *RAD53* transcript. To prepare the heat-shock samples, the cells were grown to mid log phase (OD 0.5) and divided into two batches. One batch continued to grow at 30°C, whereas the second batch of cells was exposed to 40°C for 1 h for heat-shock treatment. After 1 h, the sample was shifted to 30°C to grow for another 1 h. Equal numbers of cells were then harvested from both batches for RNA isolation. In a similar manner, cDNA was made from W303α and NKY14 to study the steady-state levels of *RAD53*. The primers OSB16 and OSB14 were used to amplify 307 base pairs at the 3′ end of the *ACT1* transcript. To amplify a 356–base pair region at the 3′ end of *CLN1*, OSB 244 and OSB 245 were used, and to amplify a 356–base pair region at the 3′ end

of *CLN2*, OSB 246 and OSB 247 were used. The 273 base pairs of *RAD53* at the 3′ end were amplified using the primer pair OSB 230–231. The RNA was isolated from *iG170Dhsp82* (temperature-sensitive strain) by growing it at 25°C (permissive temperature) and 37°C (restrictive temperature) separately. However, in case of treatment with DNA-damaging agent, *iG170Dhsp82* was grown to early log phase at 25°C and then divided into two batches. One batch continued to grow at 25°C, and the other batch was treated with 0.03% MMS for 2 h. Finally, cDNA was prepared from these fractions.

For real-time RT-PCR, cDNA was diluted (1:50) and used for PCR using a Roche RT PCR kit. Real-time analysis was done using an Applied Biosystems 7500 Fast Real Time PCR system. The threshold cycle (C_T) value of the *ACT1* transcript of each sample was used to normalize the corresponding C_T values of the desired transcripts. The normalized C_T values from different samples were compared with obtain ΔC_T values. The relative levels of mRNA were deduced from the following formula: change in mRNA level = $2^{\Delta CT}$. The mean values (±SD) from three independent experiments were plotted using GraphPad Prism 6 software.

Western blotting

Protein was extracted from W303α, NKY14, and heat-treated cells to estimate the endogenous levels of Hsp90. Before protein extraction, heat-treated samples were prepared following the same protocol as used for RNA isolation. For protein extraction upon MMS exposure, exponentially growing cells of strains NKY15, NKY16, SLY47, NKY20, NKY24, NKY28, NKY29, and NKY38 were divided into two batches. One batch was subjected to 0.05% MMS for 2 h, and the other portion continued to grow in the absence of MMS. The protein was then isolated from these two batches of each strain as described earlier (Laskar *et al.*, 2011).

UV treatment of the strains NKY15, NKY16, SLY47, NKY20, NKY24, NKY28, and NKY29 were carried out by growing them to OD 0.5, followed by making two equal parts by volume for each strain. One of the parts was subjected to a 3-kJ/m^2 dose of UV radiation and allowed to grow for 3 h posttreatment. Equal amounts of cells were finally harvested, and protein was isolated from them by the trichloroacetic acid method, followed by Western blot analysis. The antibodies used were mouse anti-Act1 antibody (Abcam, Madison, WI), rabbit anti-Rad51 (Promega), and mouse anti-Hsp82 antibody (Calbiochem, Kenilworth, NJ) at 1:5000 dilution. Rabbit anti-Myc antibody (Abcam) was used at 1:8000 dilutions. We also used anti-DDDDKK tag antibody, which recognizes Flag fusions (Abcam), and anti-Pgk1 antibody (Novus Biologicals) at 1:3000 dilution. For secondary antibodies, we used horseradish peroxidase–conjugated anti-rabbit antibody (Promega) and anti-mouse antibody (Santa Cruz Biotechnology, Dallas, TX) at 1:10,000 dilution. The Western blots were developed using a chemiluminescence detection system (Pierce, Waltham, MA). The bands on the gel were quantified using ImageJ software, and the relative densities thus obtained were plotted using GraphPad Prism software. The mean value from at least three or four independent experiments is plotted with SD. All blots are normalized against actin.

ChIP assay

The strains NA14, NA14/*Δrad51*, and NKY30 were grown to OD 0.3 in the presence of glycerol-containing medium. Each batch of cells was then divided into two parts of equal volume. One batch was allowed to continue to grow in the same way. The other batch of cells was pelleted down and resuspended in 3% galactose–containing medium for 3 h. The cells corresponding to OD 60 were then cross-linked with 1% formaldehyde at 30°C for 15 min, and the experiment was performed as mentioned earlier (Laskar *et al.*, 2015). Immunoprecipitation was performed with 1 µg of anti-Rad51 antibodies to precipitate the Rad51-bound fragment. We quantified Rad51 recruitment by PCR using donor-specific primers OSB 278 and OSB 279 in a reaction volume of 50 µl using 1/75 of immunoprecipitates and 1/50 of input DNA. Samples were subjected to electrophoresis on a 1.5% agarose. Rad51 binding was also measured at the *ACT1* locus using the primers OSB16 and OSB14. Control antibody for ChIP was rabbit immunoglobulin G. To verify that HO digestion was made in the NA14 strain, we used OSB 289 as a forward primer, which is complementary to the 20 base pairs upstream of HOcs, and a reverse primer (KanB1) that is complementary to the KANMX gene. Amplification would occur only if the galactose induction was inefficient to cause the break, whereas in the case of successful induction, no amplification would be seen. We amplified full-length *RAD51* as a control for normalization. For that purpose, we used OMKB90 and OMKB88 as forward and reverse primers, respectively.

ACKNOWLEDGMENTS

The work is supported by Grants BT/PR5739/BRB/10/1101/2012 from the Department of Biotechnology, India, to S.B. N.K. is supported by a Senior Research Fellowship from the Council of Scientific and Industrial Research, India.

REFERENCES

Abraham RT (2001). Cell cycle checkpoint signaling through the ATM and ATR kinases. Genes Dev 15, 2177–2196.

Agmon N, Pur S, Liefshitz B, Kupiec M (2009). Analysis of repair mechanism choice during homologous recombination. Nucleic Acids Res 37, 5081–5092.

Arlander SJH, Eapen AK, Vroman BT, McDonald RJ, Toft DO, Karnitz LM (2003). Hsp90 inhibition depletes Chk1 and sensitizes tumor cells to replication stress. J Biol Chem 278, 52572–52577.

Borkovich KA, Farrelly FW, Finkelstein DB, Taulien J, Lindquist S (1989). Hsp82 is an essential protein that is required in higher concentrations for growth of cells at higher temperatures. Mol Cell Biol 9, 3919–3930.

Branzei D, Foiani M (2006). The Rad53 signal transduction pathway: replication fork stabilization, DNA repair, and adaptation. Exp Cell Res 312, 2654–2659.

Caplan AJ, Jackson S, Smith D (2003). Hsp90 reaches new heights. Conference on the Hsp90 chaperone machine. EMBO Rep 4, 126–130.

Cohen Y, Dardalhon M, Averbeck D (2002). Homologous recombination is essential for RAD51 up-regulation in Saccharomyces cerevisiae following DNA crosslinking damage. Nucleic Acids Res 30, 1224–1232.

Cuadrado M, Martinez-Pastor B, Murga M, Toledo LI, Gutierrez-Martinez P, Lopez E, Fernandez-Capetillo O (2006). ATM regulates ATR chromatin loading in response to DNA double-strand breaks. J Exp Med 203, 297–303.

Daniely Y, Borowiec JA (2000). Formation of a complex between nucleolin and replication protein A after cell stress prevents initiation of DNA replication. J Cell Biol 149, 799–810.

Durocher D, Henckel J, Fersht AR, Jackson SP (1999). The FHA domain is a modular phosphopeptide recognition motif. Mol Cell 4, 387–394.

Falck J, Coates J, Jackson SP (2005). Conserved modes of recruitment of ATM, ATR and DNA-PKcs to sites of DNA damage. Nature 434, 605–611.

Finn K, Lowndes NF, Grenon M (2012). Eukaryotic DNA damage checkpoint activation in response to double-strand breaks. Cell Mol Life Sci 69, 1447–1473.

Floer M, Bryant GO, Ptashne M (2008). HSP90/70 chaperones are required for rapid nucleosome removal upon induction of the GAL genes of yeast. Proc Natl Acad Sci USA 105, 2975–2980.

Gilbert CS, Green CM, Lowndes NF (2001). Budding yeast Rad9 is an ATP-dependent Rad53 activating machine. Mol Cell 8, 129–136.

Gunjan A, Verreault A (2003). A Rad53 kinase-dependent surveillance mechanism that regulates histone protein levels in S. cerevisiae. Cell 115, 537–549.

Harrison JC, Haber JE (2006). Surviving the breakup: the DNA damage checkpoint. Annu Rev Genet 40, 209–235.

Hunt CR, Pandita RK, Laszlo A, Higashikubo R, Agarwal M, Kitamura T, Gupta A, Rief N, Horikoshi N, Baskaran R, *et al.* (2007). Hyperthermia activates a subset of ataxia-telangiectasia mutated effectors independent of DNA strand breaks and heat shock protein 70 status. Cancer Res 67, 3010–3017.

Ivanov EL, Sugawara N, Fishman-Lobell J, Haber JE (1996). Genetic requirements for the single-strand annealing pathway of double-strand break repair in Saccharomyces cerevisiae. Genetics 142, 693–704.

Jazayeri A, Falck J, Lukas C, Bartek J, Smith GCM, Lukas J, Jackson SP (2006). ATM- and cell cycle-dependent regulation of ATR in response to DNA double-strand breaks. Nat Cell Biol 8, 37–45.

Khurana N, Bhattacharyya S (2015). Hsp90, the concertmaster: tuning transcription. Front Oncol 5, 100.

Laskar S, Bhattacharyya MK, Shankar R, Bhattacharyya S (2011). HSP90 controls SIR2 mediated gene silencing. PLoS One 6, e23406.

Laskar S, Sheeba K, Bhattacharyya MK, Nair AS, Dhar P, Bhattacharyya S (2015). Heat stress induced Cup9 dependent transcriptional regulation of Sir2. Mol Cell Biol 35, 437–450.

Laszlo A, Fleischer I (2009). The heat-induced gamma-H2AX response does not play a role in hyperthermic cell killing. Int J Hyperthermia 25, 199–209.

Longtine MS, McKenzie A, Demarini DJ, Shah NG, Wach A, Brachat A, Philippsen P, Pringle JR (1998). Additional modules for versatile and economical PCR-based gene deletion and modification in Saccharomyces cerevisiae. Yeast 14, 953–961.

Mao Z, Jiang Y, Liu X, Seluanov A, Gorbunova V (2009). DNA repair by homologous recombination, but not by non homologous end joining, is elevated in breast cancer cells. Neoplasia 11, 683–691.

Marcand S, Pardo B, Gratias A, Cahun S, Callebaut I (2008). Multiple pathways inhibit NHEJ at telomeres. Genes Dev 22, 1153–1158.

Matsui T, Katsuno Y, Inoue T, Fujita F, Joh T, Niida H, Murakami H, Itoh M, Nakanishi M (2004). Negative regulation of Chk2 expression by p53 is dependent on the CCAAT-binding transcription factor NF-Y. J Biol Chem 279, 25093–25100.

Nakada D, Hirano Y, Sugimoto K (2004). Requirement of the Mre11 complex and exonuclease 1 for activation of the Mec1 signaling pathway. Mol Cell Biol 24, 10016–10025.

Nakada D, Matsumoto K, Sugimoto K (2003). ATM-related Tel1 associates with double-strand breaks through an Xrs2-dependent mechanism. Genes Dev 17, 1957–1962.

Nathan DF, Lindquist S (1995). Mutational analysis of Hsp90 function: interactions with a steroid receptor and a protein kinase. Mol Cell Biol 15, 3917–3925.

Prodromou C, Panaretou B, Chohan S, Siligardi G, O'Brien R, Ladbury JE, Roe SM, Piper PW, Pearl LH (2000). The ATPase cycle of Hsp90 drives a molecular "clamp" via transient dimerization of the N-terminal domains. EMBO J 19, 4383–4392.

Prodromou C, Roe SM, Piper PW, Pearl LH (1997). A molecular clamp in the crystal structure of the N-terminal domain of the yeast Hsp90 chaperone. Nat Struct Biol 4, 477–482.

Putnam CD, Jaehnig EJ, Kolodner RD (2009). Perspectives on the DNA damage and replication checkpoint responses in Saccharomyces cerevisiae. DNA Repair (Amst) 8, 974–982.

Sanchez Y, Bachant J, Wang H, Hu F, Liu D, Tetzlaff M, Elledge SJ (1999). Control of the DNA damage checkpoint by chk1 and rad53 protein kinases through distinct mechanisms. Science 286, 1166–1171.

Sawarkar R, Sievers C, Paro R (2012). Hsp90 globally targets paused RNA polymerase to regulate gene expression in response to environmental stimuli. Cell 149, 807–818.

Schwartz MF, Duong JK, Sun Z, Morrow JS, Pradhan D, Stern DF (2002). Rad9 phosphorylation sites couple Rad53 to the Saccharomyces cerevisiae DNA damage checkpoint. Mol Cell 9, 1055–1065.

Seno JD, Dynlacht JR (2004). Intracellular redistribution and modification of proteins of the Mre11/Rad50/Nbs1 DNA repair complex following irradiation and heat-shock. J Cell Physiol 199, 157–170.

Sidorova JM, Breeden LL (1997). Rad53-dependent phosphorylation of Swi6 and down-regulation of CLN1 and CLN2 transcription occur in response to DNA damage in Saccharomyces cerevisiae. Genes Dev 11, 3032–3045.

Siede W, Friedberg AS, Dianova I, Friedberg EC (1994). Characterization of G1 checkpoint control in the yeast Saccharomyces cerevisiae following exposure to DNA-damaging agents. Genetics 138, 271–281.

Siede W, Friedberg AS, Friedberg EC (1993). RAD9-dependent G1 arrest defines a second checkpoint for damaged DNA in the cell cycle of Saccharomyces cerevisiae. Proc Natl Acad Sci USA 90, 7985–7989.

Stecklein SR, Kumaraswamy E, Behbod F, Wang W, Chaguturu V, Harlan-Williams LM, Jensen RA (2012). BRCA1 and HSP90 cooperate in homologous and non-homologous DNA double strand break repair and G2/M checkpoint activation. Proc Natl Acad Sci USA 109, 13650–13655.

Suhane T, Laskar S, Advani S, Roy N, Varunan S, Bhattacharyya D, Bhattacharyya S, Bhattacharyya MK (2015). Both charged linker region and ATPase domain of Hsp90 are essential for Rad51 dependent DNA repair. Eukaryot Cell 14, 64–77.

Sweeney FD, Yang F, Chi A, Shabanowitz J, Hunt DF, Durocher D (2005). Saccharomyces cerevisiae Rad9 acts as a Mec1 adaptor to allow Rad53 activation. Curr Biol 15, 1364–1375.

Tariq M, Nussbaumer U, Chen Y, Beisel C, Paro R (2009). Trithorax requires Hsp90 for maintenance of active chromatin at sites of gene expression. Proc Natl Acad Sci USA 106, 1157–1162.

VanderWaal RP, Griffith CL, Wright WD, Borrelli MJ, Roti JL (2001). Delaying S-phase progression rescues cells from heat-induced S-phase hypertoxicity. J Cell Physiol 187, 236–243.

Walerych D, Kudla G, Gutkowska M, Wawrzynow B, Muller L, King FW, Helwak A, Boros J, Zylicz A, Zylicz M (2004). Hsp90 chaperones wild-type p53 tumor suppressor protein. J Biol Chem 279, 48836–48845.

Zhao X, Muller EG, Rothstein R (1998). A suppressor of two essential checkpoint genes identifies a novel protein that negatively affects dNTP pools. Mol Cell 2, 329–340.